Antarctic Science 25(4), 475–500 (2013) © Antarctic Science Ltd 2013 doi:10.1017/S0954102013000436

Synthesis
A spaceborne inventory of volcanic activity in Antarctica and southern oceans, 2000–10

MATTHEW R. PATRICK[1] and JOHN L. SMELLIE[2]

[1]*Hawaiian Volcano Observatory - US Geological Survey, PO Box 51, Hawaii National Park, HI 96718, USA*
[2]*Department of Geology, University of Leicester, University Road, Leicester LE1 7RH, UK*
mpatrick@usgs.gov

Abstract: Of the more than twenty historically active volcanoes in Antarctica and the sub-Antarctic region only two, to our knowledge, host any ground-based monitoring instruments. Moreover, because of their remoteness, most of the volcanoes are seldom visited, thus relegating the monitoring of volcanism in this region almost entirely to satellites. In this study, high temporal resolution satellite data from the Hawaii Institute of Geophysics and Planetology's MODVOLC system using MODIS (Moderate Resolution Imaging Spectroradiometer) are complemented with high spatial resolution data (ASTER, or Advanced Spaceborne Thermal Emission and Reflection Radiometer, and similar sensors) to document volcanic activity throughout the region during the period 2000–10. Five volcanoes were observed in eruption (Mount Erebus, Mount Belinda, Mount Michael, Heard Island and McDonald Island), which were predominantly low-level and effusive in nature. Mount Belinda produced tephra, building a cinder cone in addition to an extensive lava field. Five volcanoes exhibited detectable thermal, and presumed fumarolic, activity (Deception, Zavodovski, Candlemas, Bristol, and Bellingshausen islands). A minor eruption reported at Marion Island was not detected in our survey due to its small size. This study also discovered a new active vent on Mount Michael, tracked dramatic vent enlargement on Heard Island, and provides an improved picture of the morphology of some of the volcanoes.

Received 23 July 2012, accepted 23 April 2013

Key words: ASTER, fumaroles, lava-ice interaction, MODIS, satellite thermal monitoring, volcano remote sensing

Introduction

The Antarctic continent and surrounding southern oceans host more than twenty historically active volcanoes (Fig. 1, Table I), of which just two (Mount Erebus and Deception Island), to our knowledge, are monitored by ground-based instruments. For the majority, knowledge of their recent activity is incomplete due to infrequent visits. Many volcanoes in the region have been visited no more than a few times (LeMasurier & Thomson 1990). Satellite observations, although lacking the breadth and detail of information that fieldwork affords, offer the best means to routinely monitor volcanism throughout the region because of its extreme isolation. Although volcanoes in this region present little direct hazard, tracking activity there offers potential benefits in our understanding of the global sulfur budget (Gerlach 2011), volcanic effects on the sensitive polar climate (Robock 2000), impacts on fragile ecosystems (Convey & Smith 2006), and hazard processes such as lava-ice interaction (Major & Newhall 1989, Smellie & Skilling 1994, Lescinsky & Fink 2000, Edwards *et al*. 2012). Lastly, this documentation aids in maintaining the global inventory of volcanic activity (Siebert *et al*. 2010), which has broad benefits to the scientific community.

Beyond routine monitoring by the respective VAACs (Volcanic Ash Advisory Centers) for large ash clouds that might threaten flight routes, satellite imagery has played a limited role in monitoring these volcanoes, with most of the focus on the persistent lava lake at Mount Erebus (Rothery *et al*. 1988, Rothery & Oppenheimer 1994, Harris *et al*. 1997, 1999, Davies *et al*. 2008, Wright & Pilger 2008). Beyond Erebus, Lachlan-Cope *et al*. (2001) used AVHRR (Advanced Very High-resolution Radiometer) imagery to identify a recurrent lava lake at Mount Michael, on Saunders Island in the South Sandwich Islands. Patrick *et al*. (2005) used MODIS (Moderate Resolution Imaging Spectroradiometer) and ASTER (Advanced Spaceborne Thermal Emission and Reflection Radiometer) data to document the first recorded eruption of Mount Belinda, on Montagu Island, in the South Sandwich Islands. Stephenson *et al*. (2005) used high-resolution satellite imagery to document significant enlargement of McDonald Island, in the south Indian Ocean, due to recent effusive activity. As an early example of remote sensing used to monitor volcanoes in the region, questionable eruption plumes were noted in weather satellite data at Mount Siple and Webber Nunatak in 1988 and 1985, respectively (LeMasurier & Thomson 1990). But beyond

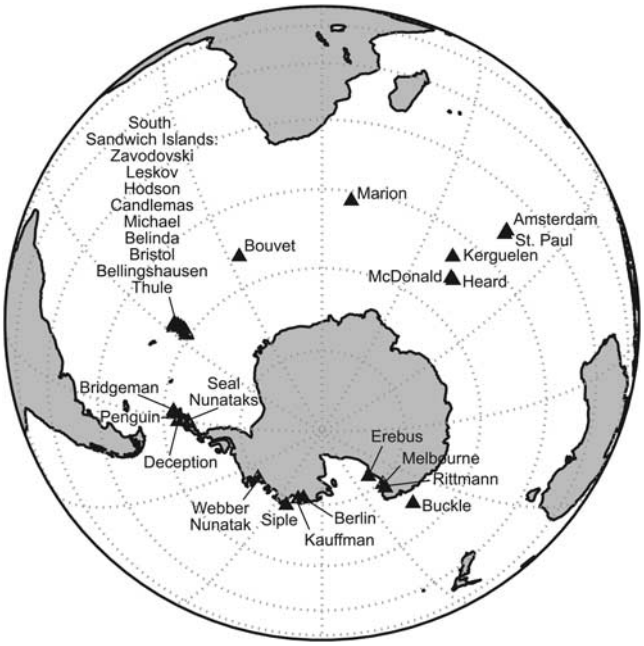

Fig. 1. General location map showing volcanoes with reported historic activity in Antarctica and the southern oceans.

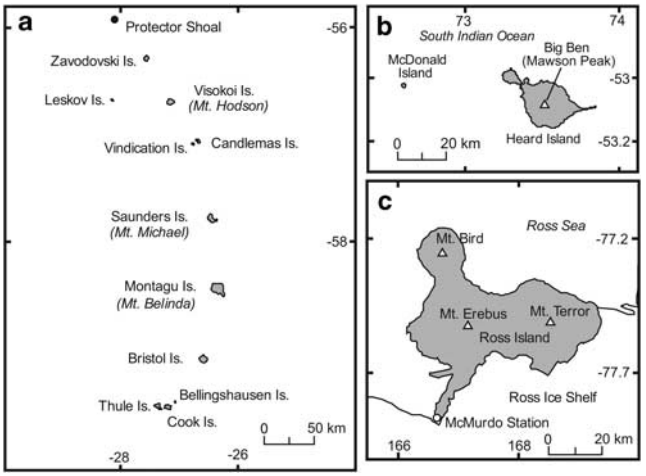

Fig. 2. Specific location maps for the volcanoes observed in eruption. **a**. South Sandwich Islands. **b**. Heard and McDonald islands. **c**. Mount Erebus and Ross Island.

these studies, satellite data have been put to little use for tracking volcanism in this region.

Robust spaceborne monitoring of the Antarctic region requires a more geographically comprehensive approach than has been used in the past. Adequate spatio-temporal coverage necessitates routine analysis of both high temporal resolution data, such as AVHRR or MODIS, and high spatial resolution imagery, such as Landsat ETM+ (Enhanced Thematic Mapper Plus) or ASTER (Harris *et al*. 1999, Dean *et al*. 2004, Patrick *et al*. 2005). Manual analysis of high temporal resolution imagery, however, can be prohibitively time consuming due to the large data volumes. Furthermore, high spatial resolution imagery has been extremely expensive (hundreds of dollars per scene) until recently. Fortunately, recent advances in automated detection of thermal anomalies in high temporal resolution data (notably the MODVOLC-MODIS system), coupled with free access to some high spatial resolution data (such as ASTER, Landsat and EO-1 ALI (Earth Observing 1 Advanced Land Imager)), now allow adequate spaceborne monitoring of remote volcanoes to be accomplished in a cost-efficient and timely manner.

In this study, we combine insights from high temporal resolution data (MODIS) and high spatial resolution data (mainly ASTER) to document the entirety of volcanic activity in Antarctica and the sub-Antarctic during the period of 2000–10. Much of the background information, including historical activity reports and volcano elevations, provided here on individual volcanoes is taken from the excellent summaries in LeMasurier & Thomson (1990). In several cases, we note where our measurements of volcanic island dimensions from the satellite images improve upon the values in LeMasurier & Thomson (1990). The dates of satellite data are shown in Co-ordinated Universal Time (UTC).

Background

Volcanoes of Antarctica and southern oceans

The Antarctic plate comprises a broad extensional province bordered almost exclusively by divergent plate boundaries, with rift-related alkaline volcanic rocks being a major constituent both on and off the continent (LeMasurier & Thomson 1990). The most active volcano in Antarctica is Mount Erebus (Fig. 2c), hosting a persistently active lava lake (Kyle 1994, Aster 2004), while Deception Island

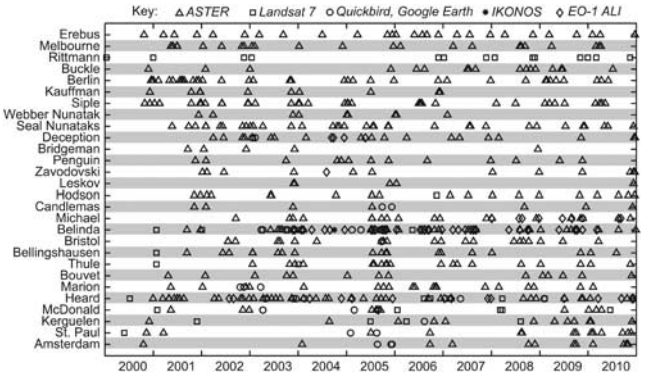

Fig. 3. Compilation of reasonably cloud-free high spatial resolution images used in the survey, covering 28 volcanoes in the Antarctic region with reported historic activity.

https://doi.org/10.1017/S0954102013000436 Published online by Cambridge University Press

Table I. List of volcanoes in this study.

Name	Lat/long	Elev. (m)	Reported activity
Antarctica and adjacent islands			
1 Erebus	-77.53, 167.17	3794	Persistent lava lake activity
2 Melbourne	-74.35, 164.70	2732	Fumarolic
3 Rittmann	-73.45, 165.50	2600	Fumarolic
4 Buckle	-66.78, 163.25	1239	Eruptions in 1839, 1899
5 Berlin	-76.05, -136.0	3478	Fumarolic
6 Kauffman (Ames Range)	-75.6, -132.4	2364	Fumarolic
7 Siple	-73.43, -126.67	3110	Unconfirmed eruption report, 1988
8 Webber Nunatak (Hudson Mts)	-74.78, -99.84	495	Unconfirmed eruption report, 1985
9 Seal Nunataks	-65.03, -60.05	350	Unconfirmed eruption report 1893
10 Deception	-62.97, -60.65	539	Fumarolic; eruptions in 1967, 1969, 1970
11 Bridgeman	-62.05, -56.75	240	Fumarolic (?)
12 Penguin	-62.10, -57.93	180	Residual heat (?)
South Sandwich Islands			
13 Zavodovski	-56.30, -27.57	551	Steaming; eruption inferred in 1830
14 Leskov	-56.67, -28.13	190	Fumarolic
15 Hodson (Visokoi Is.)	-56.70, -27.15	1005	Eruption in 1830
16 Candlemas	-57.08, -26.67	550	Fumarolic; geysers and hot pools
17 Michael (Saunders Is.)	-57.78, -26.45	990	Steaming; lava lake activity
18 Belinda (Montagu Is.)	-58.42, -26.33	1370	Eruption 2001–07
19 Bristol	-59.03, -26.58	1100	Eruptions in 1935, 1956, 1962(?)
20 Bellingshausen	-59.41, -27.08	253	Fumarolic; eruption sometime in 1968–84
21 Thule	-59.44, -27.37	725	Steaming
South Atlantic			
22 Bouvet	-54.42, 3.35	780	Fumarolic
South Indian Ocean			
23 Marion	-46.90, 37.75	1230	Eruptions in 1980, 2004
24 Heard (Big Ben)	-53.11, 73.51	2745	Episodic effusive eruptions; sporadic lava lake
25 McDonald	-53.03, 72.60	275	Eruptive activity since 1980
26 Kerguelen	-49.58, 69.50	1840	Fumarolic
27 St Paul	-38.72, 77.53	268	Fumarolic; eruption inferred around 1793
28 Amsterdam	-37.83, 77.52	881	Inferred historical eruption

has had several explosive eruptions in the last century (Smellie *et al*. 2002). In the surrounding sub-Antarctic region, Big Ben (Heard Island; Fig. 2b), McDonald Island, and Marion Island (all in the south Indian Ocean) have featured historic eruptions. A handful of other volcanoes in Antarctica and the southern oceans host active fumaroles or have been the subjects of unconfirmed eruption reports, as detailed in the individual volcano sections below. Bordering the Antarctic plate, the South Sandwich Islands include most of the subduction-related volcanoes in the study region, being dominated by tholeiitic basalts (LeMasurier & Thomson 1990, Leat *et al*. 2003). Nine of the eleven South Sandwich Islands (Fig. 2a) have volcanoes with reported activity, ranging from fumaroles to explosive eruptions (LeMasurier & Thomson 1990). Mount Belinda on Montagu Island experienced an eruption from 2001–07 consisting of low-intensity explosive activity and several effusive events detected and monitored almost exclusively by the spaceborne methods described in this paper (Patrick *et al*. 2005).

MODVOLC and ASTER satellite data

The satellite data used in this study comprised two primary datasets that are complementary in terms of spatial and temporal resolution. First, MODVOLC, developed by Wright *et al*. (2004), is an automated alert system that detects anomalous thermal activity in MODIS thermal satellite data. MODIS thermal data have a nominal pixel size of 1 km at nadir (Wright *et al*. 2004). The MODIS sensor is aboard two polar-orbiting satellites (Terra and Aqua), each acquiring two images per day at the equator, enabling MODIS to image a given spot on the Earth's surface at least four times daily. Wright & Pilger (2008) described how the converging orbits around the poles allow more frequent overpasses. Wright *et al*. (2004) described how MODVOLC is sensitive to surfaces emitting significant amounts of shortwave radiation, typically related to volcanic eruptions, forest fires and industrial activity. The latter two sources are non-existent in the Antarctic and sub-Antarctic, making interpretation of MODVOLC anomalies

https://doi.org/10.1017/S0954102013000436 Published online by Cambridge University Press

relatively straightforward. Wright *et al*. (2004) also noted that MODVOLC is limited to identifying significant eruptive activity (i.e. active lava at the surface), and is generally not capable of detecting lower temperature activity such as fumaroles.

Due to the coarse pixel size of MODIS it is not possible to characterize precisely the eruption style from MODVOLC data. The high spatial resolution of ASTER, our second primary dataset (Fig. 3), permitted investigation of the nature of any detected eruptive activity. Furthermore, ASTER data were used to detect non-eruptive thermal activity suggestive of fumaroles. ASTER data consist of visible/near infrared (VNIR: 15 m pixel size, Bands 1–3), shortwave infrared (SWIR: 30 m pixel size, Bands 4–9), and thermal infrared (TIR: 90 m pixel size, Bands 10–14) bands (Pieri & Abrams 2004). A major limitation of ASTER is the repeat period of the satellite (16 day orbital repeat period, but locations near the poles may be imaged with greater frequency), and the fact that acquisition is typically much more seldom than the repeat period because scheduling is on-demand. Another factor to note is that the SWIR bands on ASTER have been inoperative since April 2008.

Another factor limiting satellite monitoring of volcanoes in this region is persistent cloud cover. According to MODIS-derived estimates of cloud cover available in NASA's (National Aeronautics and Space Administration) Giovanni online data server, time-averaged cloud fraction during 2000–10 for much of the southern oceans from 45–65°S is $>80\%$. Coastal portions of Antarctica are clearer, but still $>50\%$. As an example, Mount Belinda has approximately 230 ASTER images available during the 2000–10 period, with only 25 (or 11%) being sufficiently cloud-free to show useful information. Tall volcanoes, however, such as Big Ben (Heard Island) or Mount Erebus, often had their summits above the cloud cover and had a higher rate of cloud-free views.

The ASTER and MODIS sensors reside onboard NASA's Terra satellite, which was launched in late 1999 and became operational on 24 February 2000. Another MODIS sensor resides on the Aqua satellite, launched in mid-2002 and operational on 12 July 2002. MODVOLC alert data are available freely on the internet (modis.higp.hawaii.edu), with the original MODIS data available free of charge from the NASA Reverb site (reverb.echo.nasa.gov). ASTER data, also available through Reverb, are free for scenes acquired over the United States and $80 for scenes elsewhere, although NASA-affiliated projects can request free access.

Other satellite data analysed

The MODVOLC and ASTER data were supplemented with several other satellite datatypes, including Landsat ETM+ (15–60 m pixel size), EO-1 ALI (10–30 m pixel size), IKONOS (1–4 m pixel size) and QuickBird internet browse images (unknown resolution - downgraded from the original 0.6–3 m pixel size, but still sufficiently high-resolution to be useful). Due to prohibitive costs of IKONOS and QuickBird, these datatypes were not gathered in a rigorous fashion. A few high-resolution images on Google Earth were also used. Google Earth has many areas covered by high-resolution imagery, presumably <4m in pixel size, as the source is often Quickbird or GeoEye.

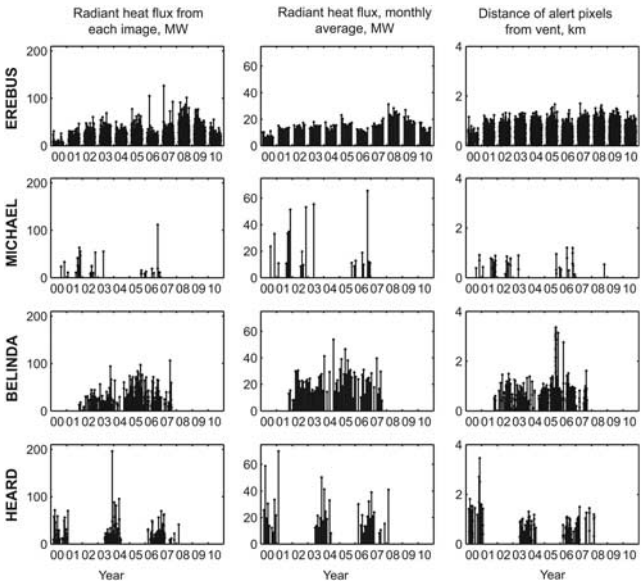

Fig. 4. MODVOLC results for radiant heat flux. Total radiant heat flux (left column) of all alert images, the monthly average of total radiant heat flux (middle column) and distance of alert pixels from the vent (right column). McDonald Island, not shown, had a single alert on 14 November 2004 which was 10 MW.

Methodology

The satellite survey consisted of two major steps: 1) a MODVOLC survey of the entire region, followed by 2) a targeted analysis of high-resolution data (ASTER etc.). The targeted analysis was limited to those volcanoes (Fig. 1, Table I) which have had: a) an observed or inferred historic eruption, b) an unconfirmed eruption report, or c) fumarolic activity, according to LeMasurier & Thomson (1990).

MODVOLC survey

The MODVOLC alert database covering the Antarctic region was examined online for the 2000–10 period. For those volcanoes with detected activity, the MODVOLC alert file, which shows dates and corresponding radiance values, was downloaded as a text file for analysis with Matlab.

Two MODVOLC-derived products are shown in Fig. 4 for the eruptive volcanoes. First, the total radiant heat flux is shown to provide a rough measure of overall activity level. The calculation of total radiant flux from the MODIS band-specific spectral radiance is based on the techniques

https://doi.org/10.1017/S0954102013000436 Published online by Cambridge University Press

described in Kaufman *et al*. (1998) and Wooster *et al*. (2003), and we specifically follow the approach in Wright & Pilger (2008). The total radiative heat flux (Φ), in Watts, can be calculated with the following equation from Wooster *et al*. (2003):

$$\Phi = 1.89 \times 10^7 (L_4 - L_{4BG}), \quad (1)$$

where L_4 is the spectral radiance (in $W\,m^{-2}\,sr^{-1}\,\mu m^{-1}$) from the alert pixel in MODIS Band 21 (3.959 μm) and L_{4BG} is the Band 21 spectral radiance of the background (i.e. areas not containing active lava). The application of this equation to MODVOLC data, and included assumptions, is described in detail in appendix A in Wright & Pilger (2008). Following Wright & Pilger (2008), the calculation is only applied to night-time data (solar zenith angles $> 90°$). Given the high latitudes of volcanoes like Erebus, this can result in periodic data gaps during the Antarctic summer. Second, we show the relative position of the MODVOLC alert pixels through time by plotting the great-circle distance to each alert pixel centre from a central point (meant to represent the vent). A simple way to calculate the central point is to use the median latitude and longitude of the volcano's entire alert dataset, as the majority of alerts tightly cluster around a central point. We limited the plot data to those scenes with a satellite zenith angle $< 30°$, as larger zenith angles lead to greatly enlarged pixels and thus greater location ambiguity (Masuoka *et al*. 1998). This plot then gives a rough idea (limited by the coarse pixel size) of how distal the alert pixels are from the central vent, enabling us to discriminate significant lava flow events from localized central vent activity.

ASTER and high-resolution data survey

ASTER data were collected for two purposes. First, the ASTER data could corroborate any MODVOLC alerts and provide a sense of the eruption style. Second, for volcanoes lacking MODVOLC alerts, the ASTER data can be searched for current fumarolic activity or the effects of any recent, unreported eruptions. We searched the online NASA Reverb archives for each targeted volcano. When fewer than 50 ASTER scenes were available in the archive for a given volcano, all scenes were visually inspected to see if they were cloud-free. For non-erupting volcanoes, when there were more than 50 scenes, we selected and analysed a manageable number of cloud-free images, aiming to have observations evenly distributed throughout the study period. For most erupting volcanoes (Mount Michael, Mount Belinda, Heard and McDonald islands) we analysed every available cloud-free image. We chose fewer images for Erebus, compared to the other erupting volcanoes, because its activity is already studied in detail by ground-based instruments. In addition, we gathered Landsat ETM+, EO-1 ALI, IKONOS and QuickBird images in a less systematic manner, focusing on the erupting volcanoes with these additional datasets. The collection of cloud-free high spatial resolution images analysed is shown in Fig. 3.

Observed activity by region

Figure 1 shows the locations for volcanoes included in this study. MODVOLC alerts occurred on five volcanoes - Mount Erebus, Mount Michael, Mount Belinda, and Heard and McDonald islands - indicating significant eruptive activity that is explored in detail below. In addition, we describe non-eruptive ASTER thermal anomalies on five volcanoes (Deception, Zavodovski, Candlemas, Bristol, and Bellingshausen islands) that suggest significant fumarolic activity.

Antarctica and adjacent islands

Mount Erebus

Mount Erebus, situated on Ross Island at the south end of the Ross Sea (Figs 1 & 2), is a large (3794 m above sea level, (a.s.l.)) stratocone with a broad caldera and a central cone hosting an active, 35 m diameter phonolite lava lake in its summit crater (Oppenheimer & Kyle 2008). The lava lake experiences occasional small strombolian bursts (Kyle 1994, Rowe *et al*. 2000). It is the best-studied and most closely monitored volcano in the region (see Kyle 1994, Aster *et al*. 2004, Oppenheimer & Kyle 2008), and is regularly visited via nearby McMurdo Station (35 km distance). Aster *et al*. (2004) described the seismic, infrasonic, GPS, infrared radiometer, gas sensor, and video equipment currently installed. These data are available via the internet in near-real-time (http://erebus.nmt.edu/).

MODVOLC indicates that magmatic activity was essentially continuous throughout 2000–10 (Fig. 4), attesting to the overall stability of the lava lake. Total radiant heat output was relatively steady between 2001 and 2006, with monthly averages around 15 megawatts (MW). This is consistent with the results of Wright & Pilger (2008) who analysed 2001–06 with the same data. A peak in radiant heat output appears to occur in 2008, when monthly averages were 20–25 MW, with a subsequent decrease over the next two years. Although the 2008 increase appears to be significant, Wright & Pilger (2008) showed how fluctuations on this scale are overshadowed by those at other lava lakes, such as Erta Ale and Nyiragongo. The overall mean radiant heat output during the study period was 17 MW. As noted in the methodology section, the periodic data gaps during the Antarctic summers are due to the lack of night-time data used for this analysis. The alert pixel locations were roughly within the location ambiguity of the MODIS pixels (~ 1 km), indicating that activity was restricted to the summit crater, as expected.

Given the excellent ground-based monitoring described above, insights from ASTER data add little to the

https://doi.org/10.1017/S0954102013000436 Published online by Cambridge University Press

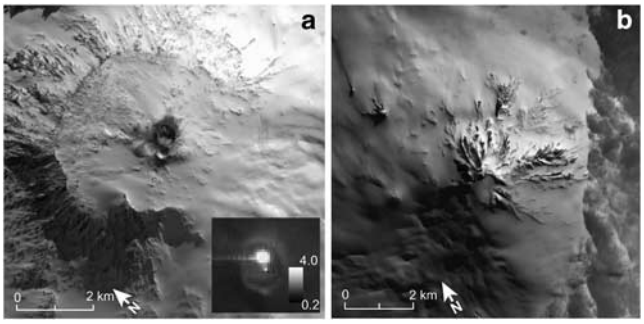

Fig. 5. a. Mount Erebus. The large image shows an ASTER (Advanced Spaceborne Thermal Emission and Reflection Radiometer) VNIR (visible/near infrared) image (Bands 3-2-1 RGB) on 9 January 2006. The inset shows the Band 9 SWIR (shortwave infrared) image of the summit crater, showing the large anomaly over Ray lava lake and a smaller adjacent anomaly to the south, in the area of Werner vent. Scale values show radiance in units of $W\,m^{-2}\,str^{-1}\,\mu m^{-1}$. The striping towards the left is presumably due to sensor saturation over Ray lava lake. **b.** Mount Melbourne. ASTER VNIR image (Bands 3-2-1 RGB) on 12 February 2006.

existing knowledge. Nevertheless, thermal anomalies were consistent with lava lake activity, being small and confined to the summit crater (Fig. 5a). Anomalies were generally 1–3 TIR pixels wide, and frequently featured saturated night-time SWIR pixels, consistent with the exposed lava that is present. The SWIR anomaly often comprised two parts, a large circular area five pixels in diameter adjacent to a smaller circular anomaly 2–3 pixels in diameter to the south. The main anomaly appears to correspond to the main lava lake (Ray lava lake (unofficial name)) and may also encompass Active vent (unofficial name), with the south anomaly in the vicinity of Werner vent (unofficial name) (Csatho *et al*. 2008, Oppenheimer & Kyle 2008).

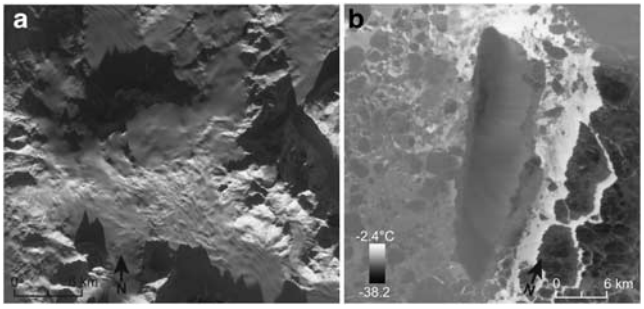

Fig. 6. a. Landsat 7 ETM+ image (Bands 3-2-1 RGB) of Mount Rittmann on 31 December 2000. **b.** ASTER (Advanced Spaceborne Thermal Emission and Reflection Radiometer) Band 14 (thermal infrared) image of Buckle Island on 13 August 2006. Scale values show at-sensor pixel-integrated brightness temperature.

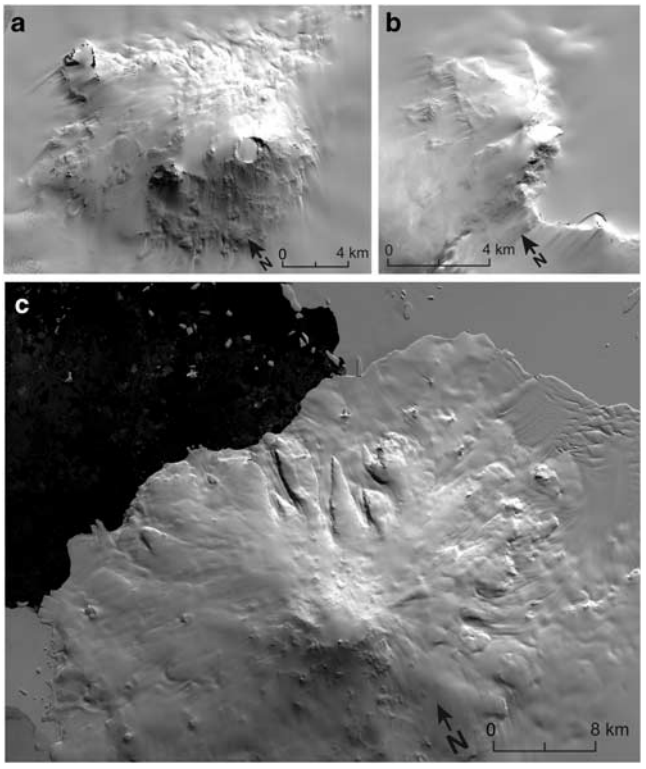

Fig. 7. a. Mount Berlin. ASTER (Advanced Spaceborne Thermal Emission and Reflection Radiometer) VNIR (visible/near infrared) (Bands 3-2-1 RGB) on 26 December 2007. **b.** Mount Kauffman, in the Ames Range. ASTER VNIR (Bands 3-2-1 RGB) on 9 December 2006. **c.** Mount Siple. ASTER VNIR (Bands 3-2-1 RGB) on 5 November 2006.

Mount Melbourne and Mount Rittmann

Mount Melbourne (Fig. 1) is a large stratovolcano (2732 m a.s.l.) on the western edge of the Ross Sea.

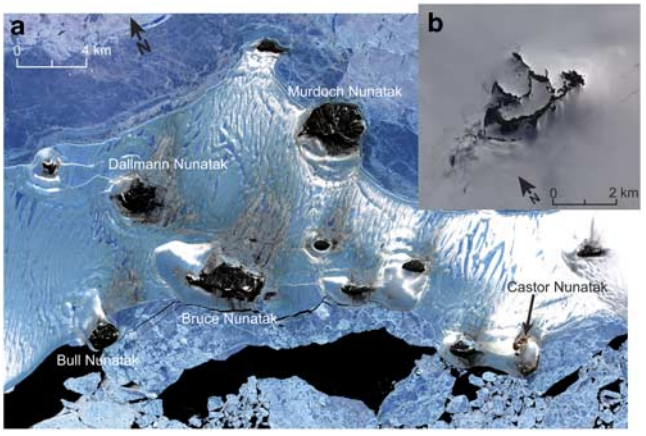

Fig. 8. a. Seal Nunataks. ASTER (Advanced Spaceborne Thermal Emission and Reflection Radiometer) VNIR (visible/near infrared) (Bands 3-2-1 RGB) on 28 October 2006. **b.** Webber Nunatak, in the Hudson Mountains. ASTER VNIR (Bands 3-2-1 RGB) on 13 January 2006.

https://doi.org/10.1017/S0954102013000436 Published online by Cambridge University Press

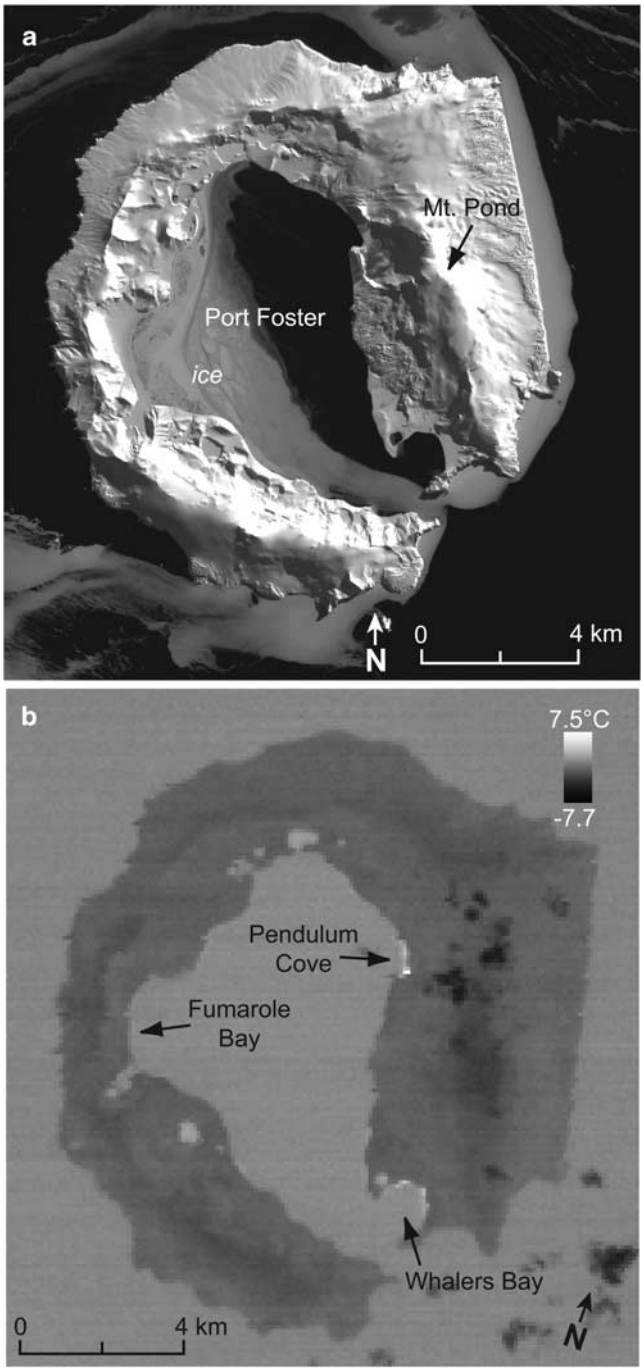

Fig. 9. Deception Island. **a.** EO-1 ALI (Earth Observing 1 Advanced Land Imager) Band 1 (panchromatic) image from 25 September 2004. The bay is partially filled with sea ice. **b.** ASTER (Advanced Spaceborne Thermal Emission and Reflection Radiometer) Band 14 (thermal infrared) image from 1 April 2006, showing shoreline thermal anomalies in Pendulum Cove and Whalers Bay, coincident with known fumarolic locations. No thermal anomalies were observed in the area of known relatively high-temperature (≥ 100°C) fumaroles in Fumarole Bay, probably as they are either too small or were below high water when the image was recorded. Scale values show at-sensor pixel-integrated brightness temperature.

Fumarolic activity has been noted at numerous locations near the summit crater, in some places producing fumarolic ice towers, and tephra distributed on and within nearby ice attest to recent (perhaps hundreds of years) eruptions, none of which have been observed (Wörner & Viereck 1989, LeMasurier & Thomson 1990). ASTER VNIR imagery shows the current areas of bare rock around the summit (Fig. 5b) correspond exactly to those shown in an 1983 aerial photograph (LeMasurier & Thomson 1990), indicating that no significant morphological changes have occurred. Accordingly, this suggests that there has not been a great change in the area of warm ground. No thermal anomalies were identified in the ASTER imagery beyond those attributed to the bare rock patches (which may be snow-free due to topography, solar heating or active heating from below). Mount Rittmann (2600 m a.s.l.) (Figs 1 & 6a) was identified as a volcanic area during Italian expeditions in the late 1980s and early 1990s when active fumaroles and heated ground were discovered (Bargagli *et al*. 1996). Small subtle thermal anomalies observed in several Landsat 7 ETM+ images may correspond to the areas of heated ground, but there was no observed change during the study period.

Buckle Island (Balleny Islands)

LeMasurier & Thomson (1990) noted that eruptions were reported at Buckle Island (Fig. 1) in 1839 and 1899, but an infrared survey in the 1960s did not identify any thermal anomalies. The few clear ASTER scenes collected show no thermal or morphological evidence for activity in our study period (Fig. 6b).

Mount Berlin, Mount Kauffman, Mount Siple

Mount Berlin (3478 m a.s.l.) contains fumarolic ice towers along the rim of its summit crater (LeMasurier & Thomson 1990). No thermal or morphological anomalies were noted in ASTER (Fig. 7a), indicating that any current fumarolic activity is below detection levels. Mount Kauffman (2364 m a.s.l.), part of the Ames Range (Fig. 7b), has weak fumarolic activity on its north flank (LeMasurier & Thomson 1990), but the ASTER imagery did not show any thermal anomalies. Mount Siple (3110 m a.s.l.) was the site of a questionable eruption report when an apparent plume was observed in satellite imagery in 1988; an overflight three months later showed no evidence of a recent eruption (Smithsonian Institution 1988a, 1988b). Despite this, the original satellite observations suggested a possible ash shadow on the snow, that the putative plume rose above the local cloud level and the plume was also observed in infrared satellite imagery (personal communication to JLS from W Gould, National Oceanic and Atmospheric Administration, 1988). Very little exposed rock was visible in ASTER imagery, and the numerous parasitic cones remained buried under snow and ice in summer (Fig. 7c).

https://doi.org/10.1017/S0954102013000436 Published online by Cambridge University Press

ASTER imagery showed no thermal anomalies or morphological indications of activity in our study period.

Webber Nunatak (Hudson Mountains)

Steaming was reported in the Hudson Mountains in 1968 (precise location unknown), and satellite imagery suggested an eruption at Webber Nunatak in 1985 (LeMasurier & Thomson 1990). Our survey shows no thermal anomalies and the morphology (Fig. 8b) is unchanged from that shown in LeMasurier & Thomson (1990). ASTER VNIR showed several instances where Webber Nunatak was entirely covered in new snow, suggesting that no substantial areas of warm ground are present.

Seal Nunataks

Several reports of activity have been made by ground observers at Seal Nunataks, including fumarolic activity, fresh tephra dispersed on the surrounding ice, and active eruptions. All the reports are considered apocryphal (LeMasurier & Thomson 1990). ASTER data show no thermal or morphological anomalies. ASTER VNIR showed an instance of complete seasonal snow cover on the nunataks, indicating that large areas of warm ground are not present. No obvious volcanic landforms could be identified with the ASTER VNIR imagery (Fig. 8a, also LeMasurier & Thomson 1990). Possible flow-like features were observed on Murdoch, Dallmann and Bull nunataks in the imagery but are unconfirmed by ground studies (Smellie & Hole 1997). A heavily eroded crater-like hollow (~ 250 m diameter) infilled by lava exists on the north side of Castor Nunatak (Fig. 8a), which is one of the few nunataks in this volcanic field built primarily of tephra. There is no evidence that it has been recently active.

Deception Island

Deception Island is a 13 km diameter horseshoe-shaped island (Fig. 9a) in the South Shetland Islands, off the northern tip of the Antarctic Peninsula (Fig. 1). Numerous small craters and cinder cones mainly reside inside the caldera rim along the inner shores, attesting to post-caldera activity. Explosive eruptions occurred in 1967, 1969 and 1970, damaging Chilean and British research stations (LeMasurier & Thomson 1990). Multiple eruptions are documented since 1783 based mainly on topographical evidence and tephra layers preserved in the island's ice cover and it contains the most complete record of historical activity of any volcano in the Antarctic and sub-Antarctic regions (Smellie *et al*. 2002). Fumarolic activity has been mapped in several locations, mainly but not solely along the inner shores (Smellie *et al*. 2002, Smithsonian Institution 2003a). The island is well-monitored seismically mainly during the Antarctic summers (Vila *et al*. 1992, Ibáñez *et al*. 2003) and it has been extensively studied (Smellie *et al*. 2002).

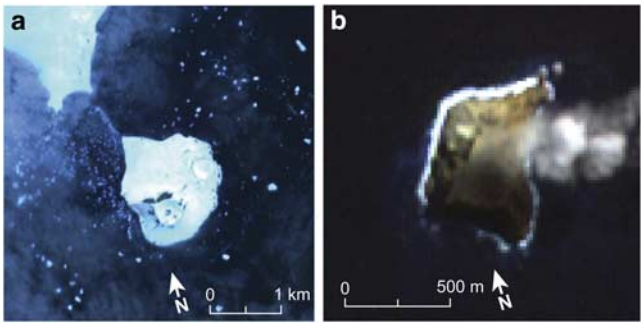

Fig. 10. a. Penguin Island. ASTER (Advanced Spaceborne Thermal Emission and Reflection Radiometer) VNIR (visible/near infrared) (Bands 3-2-1 RGB) on 19 November 2009. **b.** Bridgeman Island. ASTER VNIR (Bands 3-2-1 RGB) on 18 December 2008.

No MODVOLC anomalies were present at Deception Island, but night-time ASTER TIR imagery indicated several regions of persistent thermal anomalies suggestive of fumarolic areas (Fig. 9b). These were each only 1–3 TIR pixels in size and situated in the following locations: 1) Pendulum Cove, 2) the east shore of Whalers Bay and 3) possibly near or within the small breached tuff ring on the west side of Whalers Bay. These locations agree well with fumarole and warm ground locations mapped in the field, although no thermal anomalies were observed associated with the numerous other areas of fumarolic activity mapped on the island. These include the two highest-temperature fumaroles on the island, situated at the aptly-named Fumarole Bay. Two explanations for this are possible: 1) since most of the fumarolic fields occur between high and low tide marks, they are obscured and their temperatures masked at times of high tides (JLS, unpublished data); and 2) the majority have low measured temperatures (< 40°C; JLS, unpublished data) and the temperature contrast with unheated ground was insufficient for anomalies to be detected. By contrast, the first two sites showing thermal anomalies have temperatures of 65–75°C and the heated areas atypically (for the island) extend well above high water mark. However, a high-elevation site on the north side of Mount Pond (the highest summit on the east side of the island), measured locally at > 90°C, also does not show up. The highest temperatures at that locality are focused along narrow fractures in the rock and the heat dissipates rapidly on either side. It is likely that the size and/or average temperatures are too small to be detected easily.

Penguin and Bridgeman islands

There were no indications of any volcanic activity at Penguin Island in our study period. No thermal anomalies or anomalous areas of snow-melt were observed in ASTER imagery (Fig. 10a). The original report of possible residual

https://doi.org/10.1017/S0954102013000436 Published online by Cambridge University Press

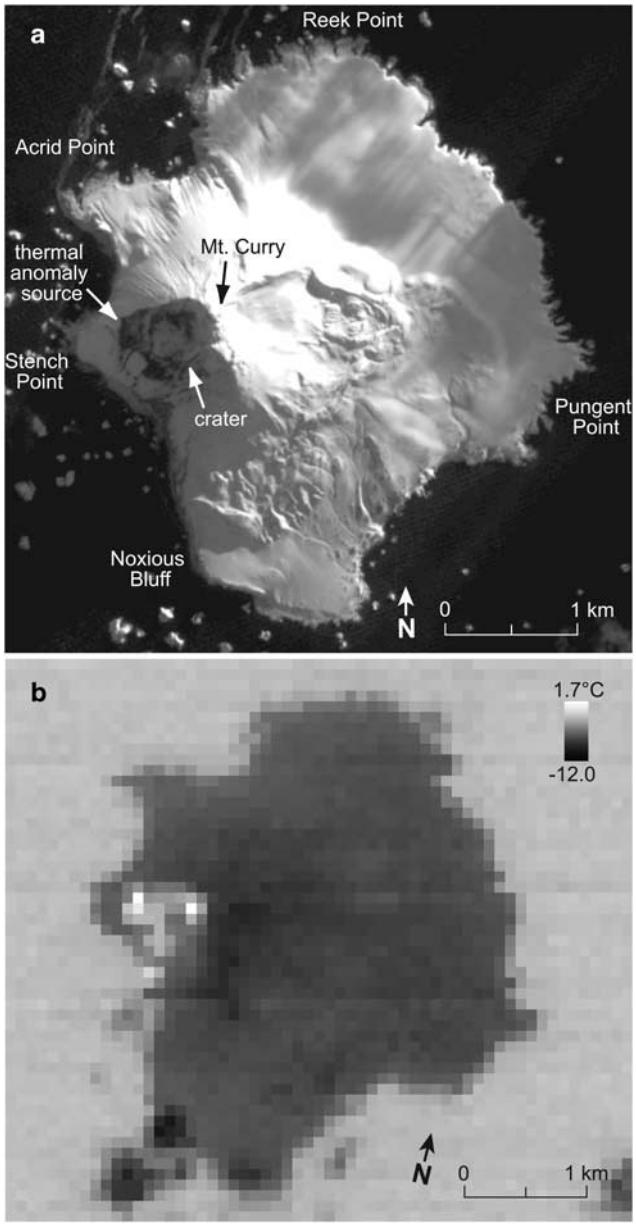

Fig. 11. Zavodovski Island, South Sandwich Islands. **a.** EO-1 ALI (Earth Observing 1 Advanced Land Imager) Band 1 (panchromatic) image from 3 August 2004. The active crater just west of the summit of Mount Curry is clearly visible. Anomalous snow-free areas on the west and south rims of the crater attest to ongoing thermal activity. A prominent sector collapse scar is also evident on the flank to the right of Mount Curry. The small inactive filled crater postulated by Leat *et al.* (2010) north-west of Mount Curry is not evident in this view. **b.** ASTER (Advanced Spaceborne Thermal Emission and Reflection Radiometer) Band 14 (thermal infrared) on 19 June 2002. Elevated temperatures are evident within the crater, and the highest temperature thermal anomaly is situated on the west rim of the crater, above Stench Point, corresponding to the snow-free zone in part a. Scale values show at-sensor pixel-integrated brightness temperature.

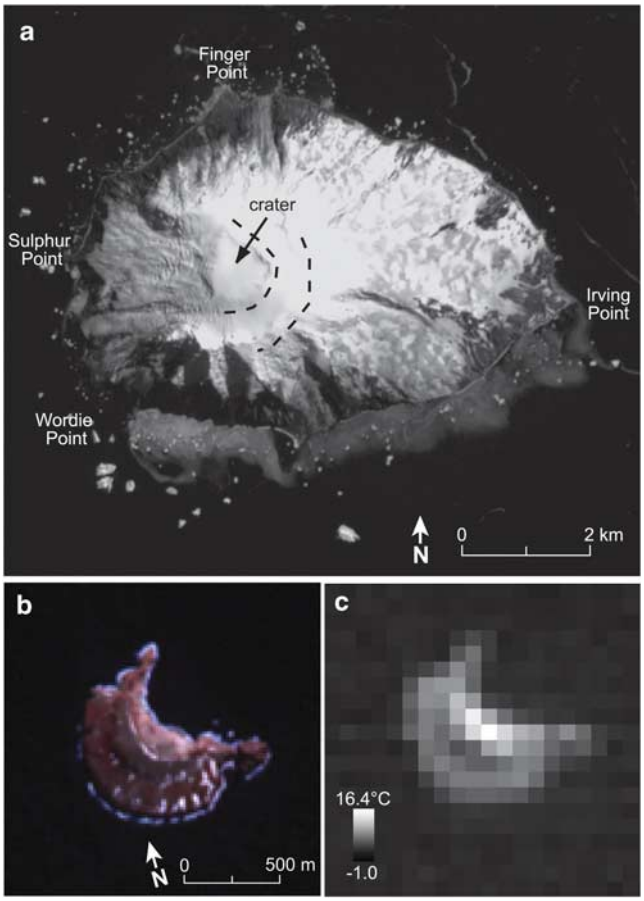

Fig. 12. a. Mount Hodson, Visokoi Island, South Sandwich Islands. Two possible nested sector collapse scars are visible, opening towards the west. The outer scar extends from Finger Point, around the summit, towards Wordie Point. A crater is situated at the head of the inner collapse scar. Landsat 7 ETM+ (Enhanced Thematic Mapper Plus) panchromatic Band 8 from 13 November 2006. **b.** Leskov Island, South Sandwich Islands. ASTER (Advanced Spaceborne Thermal Emission and Reflection Radiometer) VNIR (visible/near infrared) (Bands 3-2-1 RGB) on 10 December 2010. **c.** ASTER Band 14 (thermal infrared) of Leskov from the same date showing elevated temperatures along the summit ridge, coincident with known steaming ground. Scale values show at-sensor pixel-integrated brightness temperature.

heat on Penguin Island is also of dubious value and has not been confirmed subsequently (LeMasurier & Thomson 1990). Bridgeman Island is too small (800 x 500 m) to identify subtle thermal anomalies as it is covered by too few ASTER pixels (Fig. 10b) to establish background radiance levels. However, no heated ground has been observed in the field and the original evidence cited for volcanic heating (a seal with a burned flank) is of dubious value. Moreover, despite the unconfirmed identification of Bridgeman Island-derived tephra in a marine core in neighbouring Bransfield Strait (Smellie 1999), the rough

https://doi.org/10.1017/S0954102013000436 Published online by Cambridge University Press

morphology of the island bears no resemblance to any original volcanic structure. ASTER VNIR imagery shows the morphology of both islands is unchanged from that shown in LeMasurier & Thomson (1990).

South Sandwich Islands

Mount Curry (Zavodovski Island)

Zavodovski Island (4.4 km north–south x 3.8 km east–west) consists of a single volcanic edifice, the basaltic Mount Curry (551 m a.s.l.), which has a steeply inclined active crater oriented south-west from the summit. Notwithstanding the irregular shape of the island, our dimensions for the island are significantly different than those shown in LeMasurier & Thomson (1990), which appear to be based on the maps of Holdgate & Baker (1979). Their north-east to south-west distance is 5.5 km while ours is 3.8 km, and their north-west to south-east distance is 4.9 km while ours is 4.0 km. Our measurements are taken directly from the georeferenced satellite imagery and should therefore be more accurate.

The eastern slopes of Mount Curry comprise a broad lava platform ending in low cliffs (Fig. 11a), allowing access for both chinstrap penguins and infrequent human visitors. Intense fumarolic activity and steaming emanating from the active crater have been noted numerous times, and more rarely from the east and south coasts (the coastal examples did not exist in January 1997 (JLS, personal observation)). An eruption around 1830 was inferred from fresh-looking lava (LeMasurier & Thomson 1990) and a tall eruption column was observed by a British ship in the mid-1970s that might record a small eruption (personal communication to JLS from C. Swithinbank, British Antarctic Survey, *c.* 1995). ASTER TIR anomalies were present around the 500 m diameter crater in most clear scenes in our survey. The highest elevated pixels were located outside of the crater, on the west and south-west flanks of the active crater, towards Stench Point (Fig. 11b). Both places remain active sites of thermal emissions (observation by JLS in March 2006). A faint steam plume emanating from the crater was also visible in several scenes.

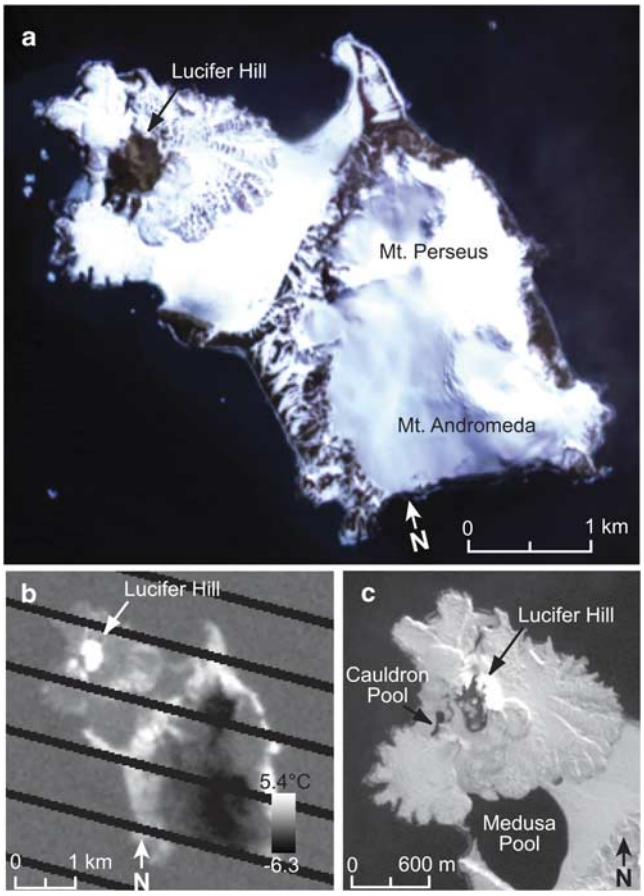

Fig. 13. Candlemas Island, South Sandwich Islands. **a.** ASTER (Advanced Spaceborne Thermal Emission and Reflection Radiometer) VNIR (visible/near infrared) (Bands 3-2-1 RGB) from 6 November 2001. A snow-free area is evident on Lucifer Hill, an area of known fumarolic activity. **b.** Landsat 7 ETM+ (Enhanced Thematic Mapper Plus) Band 6 (thermal infrared) showing the thermal anomaly at Lucifer Hill, from 13 November 2006. Scale values show at-sensor pixel-integrated brightness temperature. **c.** EO-1 ALI (Earth Observing 1 Advanced Land Imager) Band 1 (panchromatic) from 3 June 2009 showing the snow-free zone on Lucifer Hill. Also Cauldron Pool is commonly ice-free, even when Medusa Pool is frozen (cf. Fig. 13a).

Mount Hodson (Visokoi Island)

The Mount Hodson (1005 m a.s.l.) stratocone comprises the whole of Visokoi Island (5.4 x 7.7 km). The largely ice-covered volcano is basaltic in composition, and features a reported small crater at its summit as well as several basaltic scoria cones on the lower flanks. A probable eruption was observed in 1830, and a plume was also seen issuing from the summit in 1930 (LeMasurier & Thomson 1990). ASTER imagery from our study period showed no anomalous thermal features. Although the summit was masked by clouds in most scenes, a Landsat 7 ETM+ image from 13 November 2006, showed the rough morphology of the island (Fig. 12a). The western half of the island contains what appear to be two nested sector collapse scars, with the inner one hosting a 900 m wide crater at its top. An overflight in January 1997 by JLS suggested the presence of a small caldera (which might be one of the collapse scars now identified in the imagery) and a central crater, both largely snow filled and breached on the west side.

Leskov Island

Leskov Island (Fig. 12b) is the smallest of the South Sandwich Islands, just 930 x 550 m, and is situated about 50 km west of the main arc. The arcuate island is a steep eroded volcano

https://doi.org/10.1017/S0954102013000436 Published online by Cambridge University Press

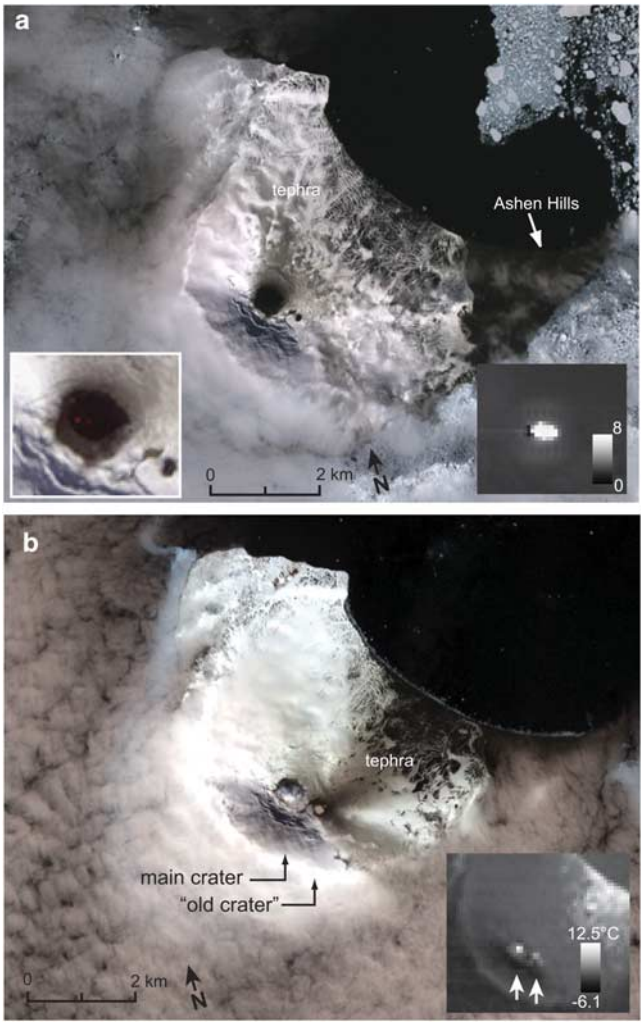

Fig. 14. Mount Michael, Saunders Island, South Sandwich Islands. **a.** ASTER (Advanced Spaceborne Thermal Emission and Reflection Radiometer) VNIR (visible/near infrared) (Bands 3-2-1 RGB) from 28 October 2006, showing active lava in the summit crater. Left inset shows two small Band 3 (near infrared) anomalies, indicative of incandescent lava at the surface. Right inset shows the Band 9 (shortwave infrared (SWIR)) anomaly, with black sensor recovery pixels and striping presumably resulting from sensor saturation over the lava surface. Scale values show radiance in units of W m^{-2} str^{-1} μm^{-1}. **b.** ASTER VNIR (Bands 3-2-1 RGB) from 17 November 2010, showing the main crater filled with steam, and recent ash emission from the crater labelled "Old Crater" by Holdgate & Baker (1979). This reactivated crater appears to be filled with steam in this image. The inset shows the Band 14 (thermal infrared) image, which has a clear thermal anomaly over "Old Crater" as well as the main crater. Scale values show at-sensor pixel-integrated brightness temperature.

remnant described as a small stratovolcano or cone, exhibiting uniform andesitic composition (LeMasurier & Thomson 1990). More recent work suggests it is a dome degraded by late-stage explosive activity (JLS, unpublished data). There has been fumarolic activity noted along the summit rim by LeMasurier & Thomson (1990). Only five cloud-free ASTER scenes were available in our study period. The ASTER VNIR images showed a snow-free region coinciding with the known fumarolic activity on the summit ridge, as well as elevated temperatures in the TIR imagery (Fig. 12c). It is not possible to say whether these higher apparent temperatures along the summit ridge are due directly to fumarolic activity or simply solar heating. A visit in January 1997 confirmed that warm ground still remains along the ridge crest (JLS, personal observation).

Candlemas Island

Candlemas Island (5.4 x 2.5 km) is composed of two major parts. The south-east region of the island consists of steep glacier-covered mountainous terrain while the north-western region is relatively low, and formed by young andesite-dacite lavas and cinder cones (Fig. 13a). Reported activity (steam emission, geysers, hot pools) has been centred around the Lucifer Hill cinder cones on the north-western side of the island (LeMasurier & Thomson 1990), but by February 1997, at least, neither hot pools nor geyser activity were evident (JLS, personal observation). ASTER and Landsat TIR anomalies were present in the central portion of Lucifer Hill in our study period (Fig. 13b), coincident with several young overlapping cinder cones. This anomalous area (~ 400 x 600 m) corresponded to a persistent snow-free zone in ASTER VNIR and EO-1 ALI visible images (Fig. 13c), which was still vigorously steaming during a March 2006 overflight (JLS, personal observation) and coincides with the location of the series of three pyroclastic cones that form Lucifer Hill. Cauldron Pool, adjacent to Lucifer Hill, also appeared anomalously ice-free in several images and may be warmed, probably by groundwater emanating from the hot ground in the summit cones directly above. One summer acquisition showed the Lucifer Hill thermal anomaly was evident regardless of the presence of snow on the island (cf. Fig. 13c).

Mount Michael (Saunders Island)

Saunders Island (9.2 x 6.3 km) is dominated by Mount Michael, a symmetric stratocone (990 m a.s.l.) topped with a 500 m wide crater that is thought to host an active lava lake (Lachlan-Cope *et al*. 2001). The volcano is largely ice-covered and predominantly basalt and basaltic-andesite in composition. The south-east portion of the island, Ashen Hills, comprises several eroded coalesced pyroclastic cones. Persistent dense steam emission has been noted from the summit of Mount Michael on numerous occasions (Holdgate & Baker 1979, LeMasurier & Thomson 1990).

MODVOLC thermal alerts have occurred sporadically during 2000–10, often separated by periods of months (Fig. 4). The alert distance indicates activity restricted to the summit crater (Fig. 14). Radiant heat flux had an overall average value of 27 MW, higher than the average of 17 MW

https://doi.org/10.1017/S0954102013000436 Published online by Cambridge University Press

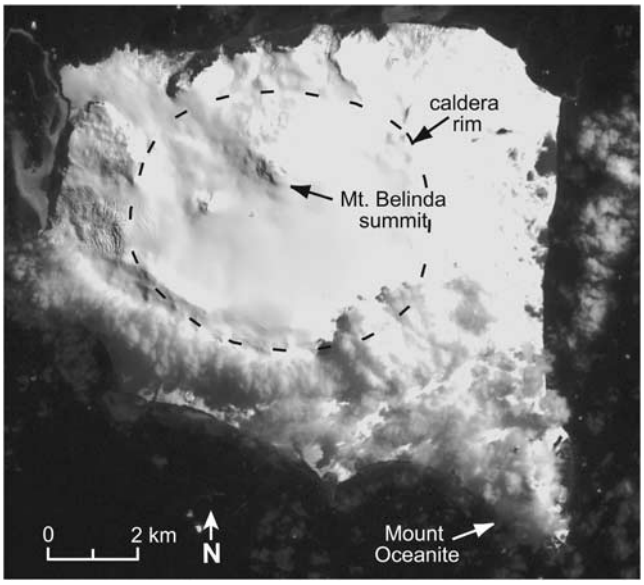

Fig. 15. Pre-eruption image of Mount Belinda, Montagu Island, South Sandwich Islands. Landsat 7 ETM+ (Enhanced Thematic Mapper Plus) Band 8 (panchromatic) image from 24 January 2001. The high point of the island, at the summit of Mount Belinda, is entirely snow-covered.

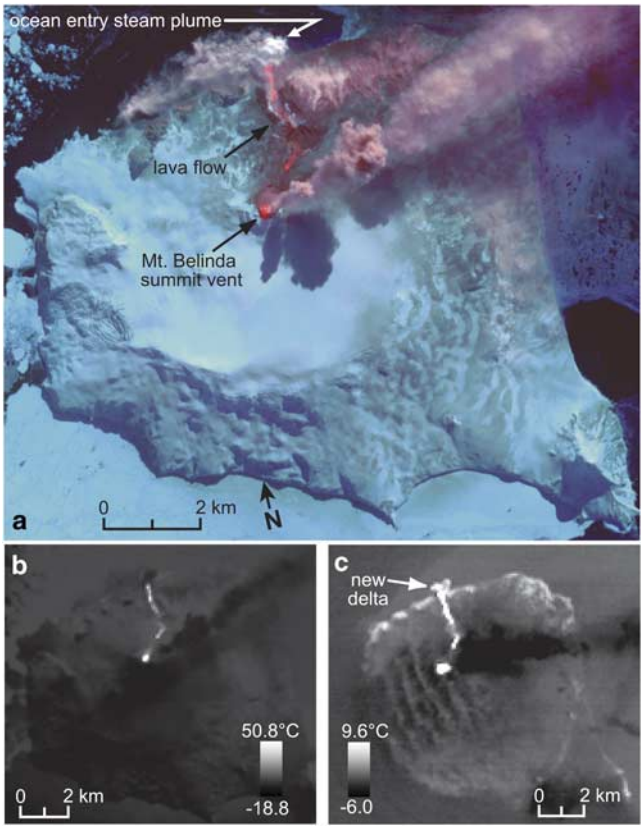

Fig. 16. Climax of Mount Belinda's 2001–07 eruption. **a.** ASTER (Advanced Spaceborne Thermal Emission and Reflection Radiometer) Bands 14-2-1 RGB (thermal infrared (TIR) and visible composite) on 23 September 2005 showing a thermal anomaly (red) at the summit of Mount Belinda, along with thermal anomalies down the path of the lava flow. The 3.5 km long lava flow was erupted from the summit and flowed to the sea. A weak ash plume is being erupted from Mount Belinda and an ocean entry plume can be seen at the coast where the lava flow is entering the water. **b.** Band 14 (TIR) image on the same date as a., highlighting the lava flow. **c.** ASTER Band 14 (TIR) image on 9 January 2006, showing the new, warm delta formed in the September–October eruptive sequence. Scale values show at-sensor pixel-integrated brightness temperature.

at Mount Erebus. ASTER images commonly showed TIR and saturated SWIR anomalies, consistently confined to the summit crater, as well as steam plumes in virtually all VNIR images. Several ASTER TIR and night-time SWIR images featured thermal anomalies at the summit region despite a lack of recent MODVOLC alerts, indicating that some activity, although muted, occurs during non-alert periods. Also, a few of the ASTER images lacked thermal anomalies at the summit, and at these times the VNIR data showed a snowy, fume-filled crater.

Figure 14a shows one of the clearest ASTER images over Mount Michael, from 28 October 2006 (Smithsonian Institution 2006a), and this is roughly coincident with a cluster of MODVOLC alerts on 20–21 October. The image shows the 500 m diameter main summit crater containing two small anomalies in the Band 3 data (near-infrared, 0.8 μm), most likely indicating exposed, incandescent lava. In addition, a large SWIR anomaly (Fig. 14a) with saturated pixels was situated within the crater, further attesting to the presence of active lava in the crater. A faint dark blanket extends out from the main summit crater onto the upper north-east slope, indicating minor ash fall from the plume and attesting to weak explosive activity (Fig. 14a).

ASTER imagery also provides new information on the small subordinate crater, marked as "Old Crater" by Holdgate & Baker (1979), presumably because it was inactive at the time of their observations. The 28 October 2006, ASTER image shows an apparent SWIR anomaly at "Old Crater", and the crater itself appears snow-free and is *c.* 150 m in diameter. An ASTER image from 5 January 2008, shows an obvious steam plume coming from this vent, which appears to be about 190 m wide, and a TIR anomaly. A very high-resolution image from November 2009 available on Google Earth shows a small steam plume emanating from the crater, which is about 190 m wide. An ASTER image from 17 November 2010 (Fig. 14b), shows apparently recent eruptive activity in "Old Crater", evidenced by tephra fallout emanating from the crater and a small TIR anomaly (at the time there was also a TIR anomaly in the main crater). The plume, tephra fall, SWIR anomalies and crater enlargement (from 150–190 m) indicate that this vent had reactivated by late 2006.

https://doi.org/10.1017/S0954102013000436 Published online by Cambridge University Press

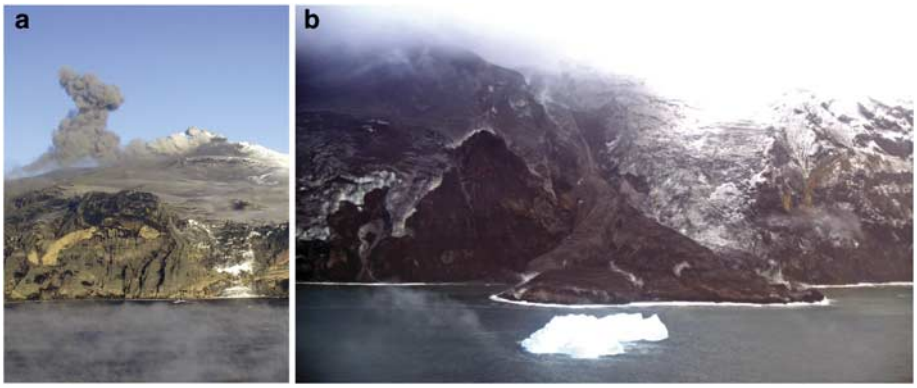

Fig. 17. Photographs of Mount Belinda. **a.** View from north of the island, showing a weak ash-laden plume erupting from the cinder cone at the summit of Mount Belinda, surrounded by tephra-covered ice. Photo by Rob Ashurst, Royal Air Force, August 2006. **b.** View of the 800 m wide lava delta formed in September–October 2005, fed by a steep channelized block lava flow cascading down the sea cliff. The delta was inactive at this time, and has two main lobes. The final subsidiary extrusion of lava is seen just entering the small new lagoon at left side (behind steam). It terminated without advancing far into the sea (cf. Fig. 20a). Photo by JLS, March 2006.

The MODVOLC and ASTER data together indicate highly sporadic activity at Mount Michael during 2000–10. The activity ranges from periods with no MODVOLC alerts and a snowy, fume-filled crater and no ASTER SWIR anomaly to brief periods with several MODVOLC alerts and lava visible in the crater. Very likely, this reflects fluctuating levels in the summit lava lake, as also postulated by Lachlan-Cope *et al*. (2001). Potential analogues in terms of morphology and activity include Villarrica Volcano, Chile (Calder *et al*. 2004), and Shishaldin Volcano, Alaska (Dehn *et al*. 2002), where the active lava has a fluctuating depth in the conduit and a variable surface crust, both of which would strongly affect the MODIS signal. The higher level of radiant heat flux at Mount Michael, compared to Mount Erebus, is likely due to the larger lava lake at Mount Michael, which appeared to be filling much of the 500 m diameter crater when it was active in October 2006 (Fig. 14a).

Mount Belinda (Montagu Island)

Montagu Island (11 x 12 km) features a broad 6 km wide ice-filled caldera topped by a relatively small intracaldera volcanic cone, Mount Belinda (1370 m a.s.l.) (Fig. 15). A prominent parasitic centre, Mount Oceanite, comprises the south-east promontory of the island. The few samples collected are basalt to basaltic-andesite in composition. Prior to 2001, there was no record of Holocene activity (LeMasurier & Thomson 1990), but as with all volcanoes in the region the record is limited by scant observations and few ice-free exposures. An overflight in January 1997 revealed no signs of recent activity (JLS, personal observation).

The first recorded eruption of Mount Belinda began sometime between 10 September and 20 October 2001, according to ASTER (a non-eruptive image was collected on 10 September) and MODVOLC (the first thermal alert occurred on 20 October, Fig. 4) (Smithsonian Institution 2003b, Patrick *et al*. 2005) and the eruption ended in September 2007 (Smithsonian Institution 2008), amounting to six years of continuous activity. Low-intensity explosive activity, several effusive events, and a persistent steam-ash plume characterized the eruption.

Several effusive events were detected in high-resolution imagery (ASTER, Landsat and EO-1 ALI). First, a small lava flow from late 2001 or early 2002 was 600 m long by 200 m, extending from the summit vent. A second, much larger lava flow was emplaced by March 2003, but its exact date is poorly constrained (Patrick *et al*. 2005). The lava extended 2 km north and carved a gully into the ice cover. The lava abutted a north-trending ridge and the front spread to 500 m wide, and the ice cover surrounding the flow showed deep crevasses radiating out from the flow margin,

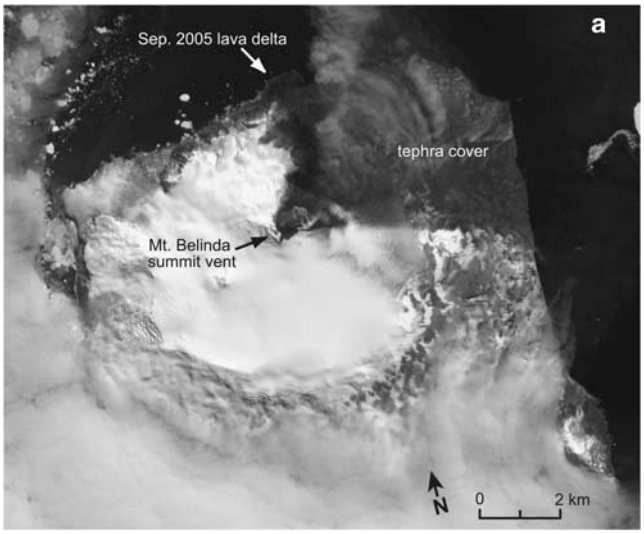

Fig. 18. Mount Belinda erupting. ASTER (Advanced Spaceborne Thermal Emission and Reflection Radiometer) VNIR (visible/near infrared) (Bands 3-2-1 RGB) from 28 October 2006, showing a weak ash plume erupting from the summit of Mount Belinda, and extensive tephra cover on the north-east portion of the island. The delta formed in September–October 2005 can be seen on the north coast.

https://doi.org/10.1017/S0954102013000436 Published online by Cambridge University Press

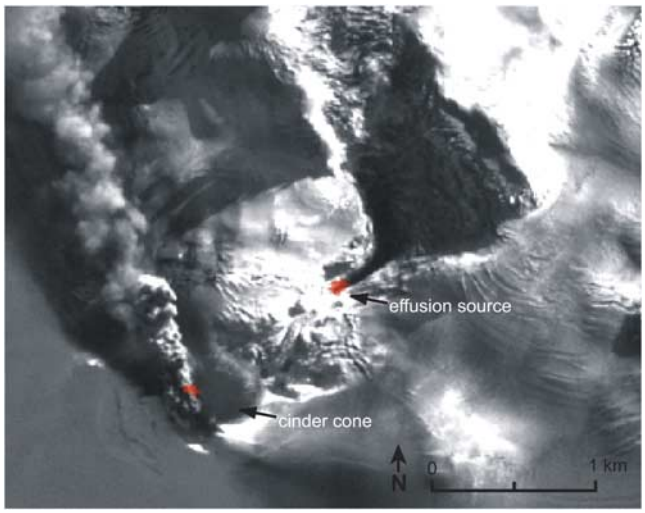

Fig. 19. Mount Belinda cinder cone and effusion source. EO-1 ALI (Earth Observing 1 Advanced Land Imager) Band 1 (panchromatic) image with the Band 10 (shortwave infrared (SWIR)) thermal anomalies overlain in red, acquired on 16 July 2005. A narrow ash plume is seen originating from the vent, which has built a cinder cone 500 m wide with a crater 150 m in diameter. A small SWIR thermal anomaly is visible near the top of the cinder cone. Additionally, a thermal anomaly is situated 1.1 km north-east of the main vent, which appears to be the source of lava effusion, feeding flows into the north-trending valley.

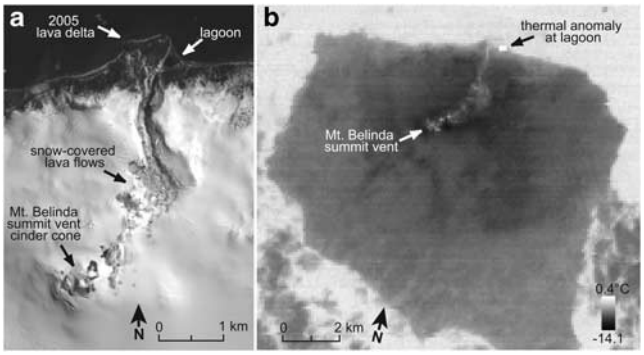

Fig. 20. Mount Belinda post-eruption. **a.** EO-1 ALI (Earth Observing 1 Advanced Land Imager) Band 1 (panchromatic) image from 20 November 2009, spanning the vent to the ocean. Most of this route is snow-covered, including the summit crater on the cinder cone. Several snow-free patches can be seen on the cinder cone, probably attesting to some minor residual heat. A small lagoon can be seen at the east margin of the 2005 lava delta, flanked by a beach bar. The lagoon coincides with a persistent post-eruption thermal anomaly suggesting influx of meltwater heated by lava, which was still cooling at that time. **b.** ASTER (Advanced Spaceborne Thermal Emission and Reflection Radiometer) Band 14 (thermal infrared) image from 21 March 2010, showing minor thermal anomalies between the vent and the ocean, along the route of lava flows emplaced between 2001 and 2007, reflecting some residual heat. A thermal anomaly is coincident with a lagoon in front of the final termination of the 2005 lava delta. Scale values show at-sensor pixel-integrated brightness temperature.

suggesting the ice was quite deep. Third, the largest effusive event of the eruption (in terms of flow length) occurred in late September 2005 (Smithsonian Institution 2005a). Lava followed the northerly path of the second lava flow, presumably overplating it, and reached the sea at 3.5 km distance (Fig. 16a). A 23 September 2005, ASTER image showed a SWIR anomaly at the summit vent, with a weak ash plume drifting north-east. Approximately 1 km north-east of the summit vent, a SWIR anomaly marks what appears to be the source of the lava, suggesting either that a secondary vent is in action or the flow is crusted over from the summit to this point. The latter possibility is more likely as the Mount Belinda summit crater was full of lava at the time. The TIR anomaly extends to the sea, where a white ocean entry plume is visible (Fig. 16a). A cluster of anomalously distal MODVOLC alerts occurred between 13 September and 1 October 2005, suggesting that this effusive episode spanned this period and lasted two to three weeks. A 16 October 2005, EO-1 ALI image shows a new delta built by this effusive episode, measuring 800 m wide along shore, extending out 500 m, and composed of two distinct lobes (see also Smithsonian Institution 2005b, Fig. 16c). Montagu Island was visited in January 2006 by the South African ship *SA Agulhas* (Smithsonian Institution 2006b), by author JLS in March 2006, and by the Royal Air Force in August 2006. Photos of the island from these visits show a cinder cone at the top of Mount Belinda (Fig. 17a) surrounded by ash-covered ice and a steep, narrow channelized block lava flow emerging from the ice cover and flowing down the sea cliff, forming the steep-faced, steaming delta (Fig. 17b).

MODVOLC and EO-1 ALI imagery indicate that additional effusive events occurred after September 2005, but all appear to have been brief. Distal MODVOLC alert pixels also occurred on 18 November 2005, and 17 March 2006 (Fig. 4), suggesting additional long, but brief, flows were emplaced after the September 2005 episode. An EO-1 ALI image appears to show an active, or recently active, short flow within about a kilometre of the summit vent in August 2006, and an ASTER image from October 2006 shows a flow extending at least 800 m. Also, clear views in EO-1 ALI imagery in July 2007 show what appear to be several short, narrow lava flows that were emplaced since August 2006. Alternatively, these events might simply indicate breakouts from local tumuli caused by lava freezing at the flow front and lava, still slowly effusing from the crater, backing up and ultimately bursting out onto the surface.

In addition to effusive events, low-intensity explosive activity in the summit crater was evidenced by the common

https://doi.org/10.1017/S0954102013000436 Published online by Cambridge University Press

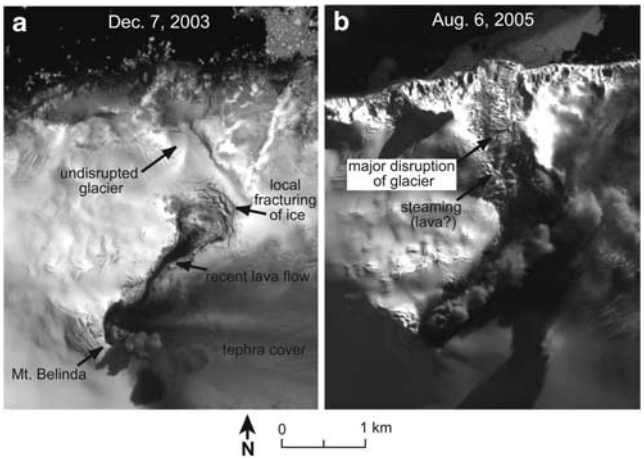

Fig. 21. Disruption of the ice cover on Mount Belinda. **a.** This EO-1 ALI (Earth Observing 1 Advanced Land Imager) Band 1 (panchromatic) image from 7 December 2003 shows the ice cover north of the flow field to be relatively undisturbed. **b.** The EO-1 ALI Band 1 (panchromatic) image from 6 August 2005 shows increasing disruption of the ice north of the flow field, possibly due to enhanced flow of basal meltwater released by heat supplied by the lava destabilizing the overlying ice. This route was later overrun by lava entering the ocean, erupted in late September 2005.

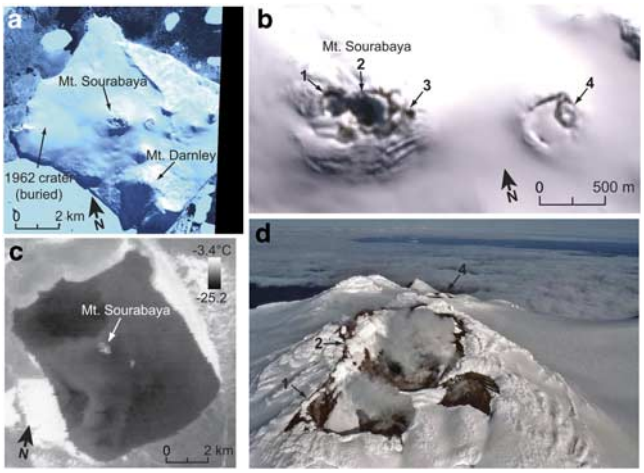

Fig. 22. Bristol Island, South Sandwich Islands. **a.** ASTER (Advanced Spaceborne Thermal Emission and Reflection Radiometer) VNIR (visible/near infrared) (Bands 3-2-1 RGB) from 23 September 2005, showing the basic layout of the island. The location where a crater and fissure was observed in 1962 is now entirely covered in snow and ice. **b.** Close-up of Mount Sourabaya, and a lower relief, unnamed crater *c.* 1 km to its east. ASTER VNIR (Bands 3-2-1 RGB) image from 28 October 2006. The composite crater at the top of Mount Sourabaya is snow-free, and exhibits a persistent thermal anomaly. Three craters (numbers 1–3) were observed at the summit of Sourabaya on a January 1997 visit, and a fourth crater (number 4) east of Sourabaya was also observed. **c.** ASTER Band 14 (thermal infrared) image from 24 July 2009, showing the persistent thermal anomalies in the summit crater of Mount Sourabaya and the unnamed crater 1 km to its east. Scale values show at-sensor pixel-integrated brightness temperature. **d.** Photo, looking east, of Mount Sourabaya summit taken by author JLS in January 1997. Numbered craters correspond with image in c. above. Crater 3 is out of view behind crater 2.

tephra cover on the eastern (downwind) side of the island (highly visible on the snow cover, Fig. 18), numerous small tephra-laden plumes seen in ASTER and EO-1 ALI imagery, and a 500 m wide cinder cone constructed over the main vent at the summit of Mount Belinda. The cinder cone was first visible in a July 2005 EO-1 ALI image (Fig. 19), and post-eruption images show that the cinder cone hosted a 150 m wide summit crater. Based on these observations, this low-level explosive activity at the summit was probably strombolian in nature and scale.

Two features - including the prominent degassing plume (often white) and circular SWIR anomaly - were consistent throughout the six-year-long eruption and, taken together, indicate that lava remained at a high level in the conduit through the eruption, probably sustained by some degree of magmatic convection.

The last MODVOLC alert was on 20 September 2007 (Fig. 4), suggesting that significant eruptive activity ended around that time. EO-1 ALI images contained SWIR anomalies at the summit vent and eruptive plumes as late as 7 September 2007. EO-1 ALI and ASTER images from May and July 2008, however, confirmed that the eruption had ended. There was no SWIR anomaly at the summit in these images, and much of the cinder cone and lava flow field were covered in snow (Smithsonian Institution 2008).

ASTER images between 2008 and 2010 show only minor TIR thermal anomalies, consistent with warm, cooling lava. The visible imagery from ASTER and EO-1 ALI shows the cinder cone and flow field becoming increasingly buried by snow through this time (Fig. 20a). In several cases, a distinct ASTER TIR anomaly is visible on the east end of the September 2005 lava delta where the final lava flow lobe terminated at the head of the small lagoon created by one of the two earlier much larger lobes (Smithsonian Institution 2010a) (Fig. 20b). An EO-1 ALI image from November 2009 shows that the small lagoon was impounded by a narrow bank of material, a likely beach bar probably at least partly sourced from erosion of the delta by wave action (Fig. 20a). The TIR anomaly may result from the confined lagoon water being warmed by residual heat from the thick delta or by a continued influx of warm water derived from melted snow and ice higher on the island and heated by the slowly cooling lava there.

MODVOLC indicates that radiant heat flux had an overall mean of 24 MW (Fig. 4). The September 2005 effusive event is shown clearly by alert pixels reaching

https://doi.org/10.1017/S0954102013000436 Published online by Cambridge University Press

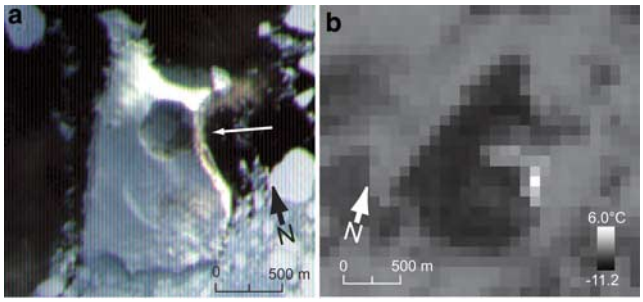

Fig. 23. Bellingshausen Island, South Sandwich Islands.
a. ASTER (Advanced Spaceborne Thermal Emission and Reflection Radiometer) VNIR (visible/near infrared) (Bands 3-2-1 RGB) on 1 August 2003. The arrow points to the location, outside of the main crater, where intense fumarolic activity was observed in 1997 (JLS, personal observation).
b. ASTER Band 14 (thermal infrared) from 28 July 2002 showing elevated temperatures within the crater and along the sea cliff on the east crater rim. Scale values show at-sensor pixel-integrated brightness temperature.

~3.5 km from the vent, however no anomalously distant pixels are present in the timeframe of the second, 2 km long, flow (Fig. 4). There has been a conspicuous steam/tephra plume in all high-resolution images collected throughout the eruption, and this coupled with the regular MODVOLC alerts strongly suggests sustained shallow magmatic activity in the Mount Belinda summit crater, possibly indicating the establishment of a lava lake, similar to that proposed for Mount Michael (Lachlan-Cope *et al*. 2001).

As lava flows were emplaced north of the Mount Belinda summit, disruption of the ice cover occurred. In ASTER VNIR images from 2003 and 2004, no apparent disruption of the glacier was evident (Fig. 21a). A July 2005 image, however, appears to show increased crevassing and morphological changes, and this was also apparent in August 2005. By September 2005 the lava flow had reached the ocean, melting ice along this route (Fig. 21b). The disruption in July and August suggests that increased activity near and around the vent (e.g. short lava flows) was driving increased melting of the ice and was a possible prelude to the September 2005 effusive episode.

Bristol Island

Bristol Island (10.5 km north–south x 10.9 km east–west), comprises a complex edifice of several overlapping volcanic centres (Fig. 22a). Note our stated dimensions are smaller than the 14 x 12 km mentioned in Holdgate & Baker (1979) and LeMasurier & Thomson (1990). The measurements in our study are directly from georeferenced satellite images and should be more accurate. The highest point, Mount Darnley (1100 m a.s.l.) is 3 km south of Mount Sourabaya, the second highest point on the island. Like Montagu Island, Bristol Island is almost entirely ice-covered, and the few samples collected indicate basaltic to andesitic compositions. An eruption in 1935 was observed at a "central peak" (which Holdgate & Baker (1979) supposed was Mount Darnley). A second eruption was witnessed in 1956, described as "three jets of glowing material". The vents responsible for these two eruptions are unknown but an overflight in January 1997 discovered three coalesced fresh-looking and steaming pyroclastic cones comprising Mount Sourabaya plus a fourth snow-filled cone, still warm but lacking steam, situated about 1.4 km east of Sourabaya (Fig. 22b & d). It is tempting to ascribe the 1935 eruption to the single crater and the three cones to the multiple-jet 1956 eruption. Finally, a steaming crater and fissure on the lower western flank of Mount Sourabaya was observed in 1962 (Holdgate & Baker 1979). The crater was measured to be 220 m wide and 60 m deep. Although identified with the 1956 eruption by Holdgate & Baker (1979), the relatively fresh appearance of the crater, presence of black ash on the surrounding ice, and the rapid ease with which temperate ice flows and recovers around an eruption site (cf. Gudmundsson *et al*. 2002) suggest to us that the eruption responsible may have taken place much closer to 1962. It is unclear from the description by Holdgate & Baker (1979) whether the crater was still present in 1964, but they noted that the fissure and ash were less conspicuous at that time. These observations suggest that the site was healing over quite rapidly and they are consistent with our suggestion of an age close to 1962.

ASTER TIR anomalies were present at the summit of Mount Sourabaya in all clear scenes (Fig. 22c). These thermal anomalies correspond to a persistent snow-free zone, in ASTER VNIR imagery, comprising the interior of the 300 x 600 m compound summit crater. In addition, another smaller snow-free zone (and resultant thermal anomaly) appears to be present in the small unnamed crater 1.4 km east of Mount Sourabaya (Fig. 22b). The thermal activity, along with the multiple craters at its summit, suggest that Mount Sourabaya was the source of the 1935 and 1956 eruptions, as opposed to Mount Darnley, which is draped by snow and ice and lacks any obvious summit crater. There were no morphological or thermal anomalies in the stated region of the "1962" vent and associated fissure, and several perfectly clear ASTER and QuickBird images indicate the crater and fissure are now completely buried under snow and ice (Fig. 22a).

Bellingshausen Island

Bellingshausen Island is a small (1.7 x 1.2 km), low-lying (253 m a.s.l.) neighbour to Thule and Cook islands (Figs 2 & 23a). The island comprises a basaltic-andesite stratocone with a 450 m diameter crater, and a relatively young lava flow field forming the southern portion of the island. Vigorous fumarolic activity was noted inside the crater as well as on its south flank by Holdgate & Baker (1979). No historic eruptions are mentioned in LeMasurier & Thomson (1990),

https://doi.org/10.1017/S0954102013000436 Published online by Cambridge University Press

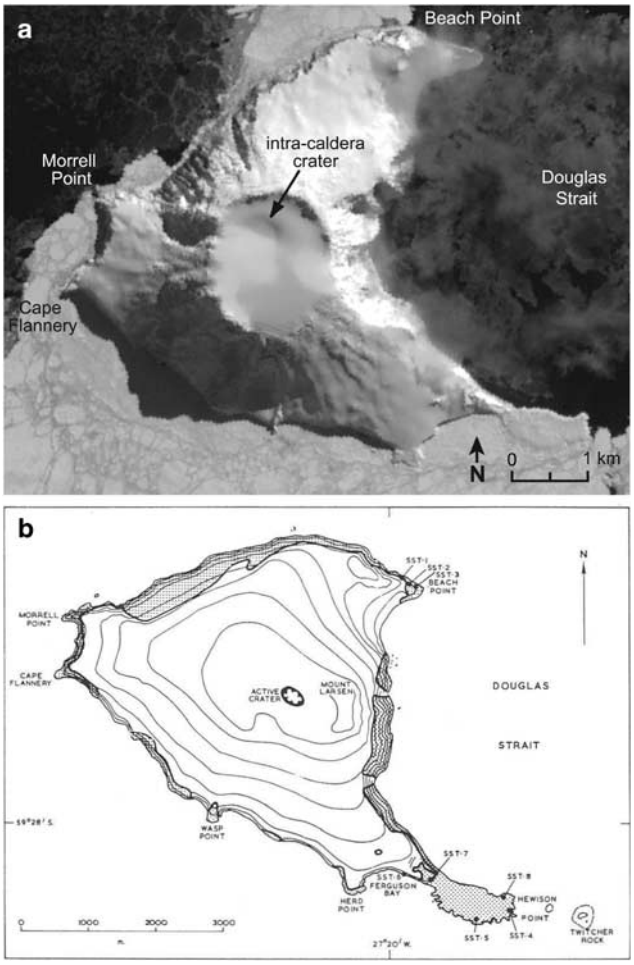

Fig. 24. Thule, South Sandwich Islands. **a.** ASTER (Advanced Spaceborne Thermal Emission and Reflection Radiometer) Band 3 image from 23 September 2005. The northern edge of a snow-filled crater, 500 m in diameter is evident as an ice-filled dimple in the northern portion of the 1.7 km wide summit caldera. The arcuate left margin of Douglas Strait, separating Thule Island from Cook Island, is the subaerial rim of a very young submarine caldera (Smellie *et al*. 1998). **b.** The map by Holdgate & Baker (1979) for reference, showing obvious differences in the shape of the island with the satellite imagery, presumably due to the rough nature of the original mapping. Map used with permission of the British Antarctic Survey.

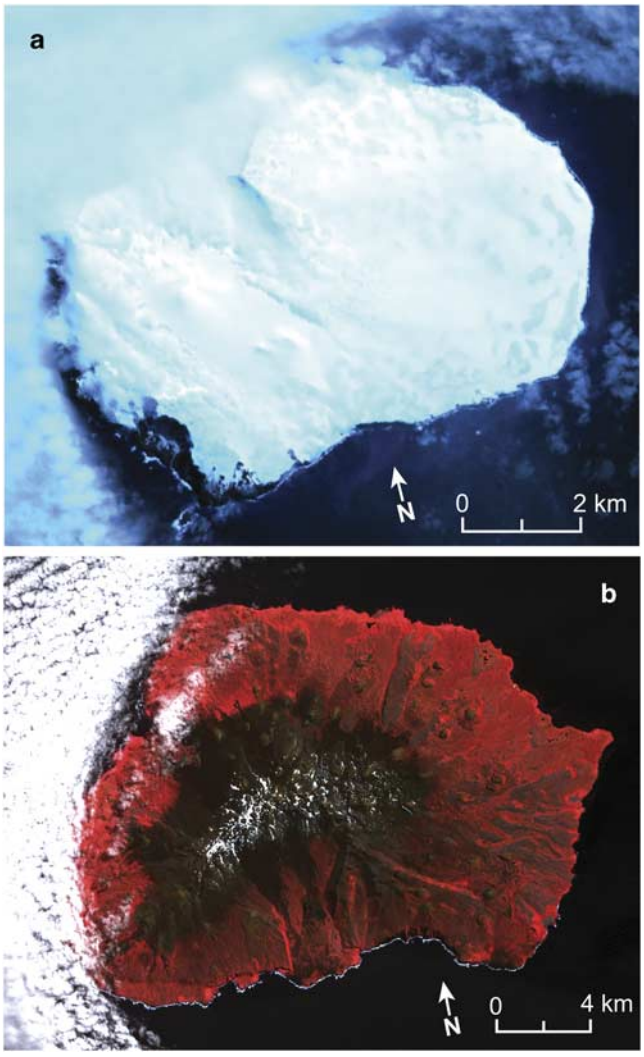

Fig. 25. a. ASTER (Advanced Spaceborne Thermal Emission and Reflection Radiometer) VNIR (visible/near infrared) (Bands 3-2-1 RGB) of Bouvet Island on 26 November 2010. **b.** ASTER VNIR (Bands 3-2-1 RGB) image of Marion Island on 26 February 2008.

although Smellie *et al*. (1998) noted that a small explosion crater formed on the south flank sometime between 1968 and 1984. Observations in January 1997 by JLS showed several slightly superheated fumaroles within the crater but only slightly warm ground in the southern areas mapped by Holdgate & Baker (1979). There was additional active steaming situated outside of the main crater on the east slopes of the island (JLS, personal observation). ASTER TIR anomalies were present in and around the central crater, along the eastern shore of the island, in all scenes in our survey (Fig. 23b). ASTER VNIR imagery showed this area to be anomalously snow-free (Fig. 23a). No thermal anomalies and only a potentially faint snow-free region were observed on the south flank, where Holdgate & Baker (1979) noted a fumarole field, indicating this field is less intense and widespread than the intra-crater field, consistent with the 1997 field observations.

Thule Island

Thule Island (6.7 x 5.3 km) forms the western flank of a fresh-looking 4 x 5 km submarine caldera underneath Douglas Strait discovered in 1997 (Smellie *et al*. 1998), with Cook Island comprising the eastern rim (Fig. 2). LeMasurier & Thomson (1990) noted that Mount Larsen, just east of the active crater in the 1962 map, forms the

https://doi.org/10.1017/S0954102013000436 Published online by Cambridge University Press

highest point (725 m a.s.l.). Samples collected include basalt, andesite and dacite (LeMasurier & Thomson 1990). Steam was observed emanating from a small water-filled summit crater in 1962 (LeMasurier & Thomson 1990). ASTER imagery in this study shows a 1.7 km wide ice-filled summit caldera (first described by Smellie *et al.* 1998) and a hint of the north rim of a small intra-caldera crater, also snow-covered (Fig. 24a). There is no indication of thermal activity, ponded water or active steaming in the summit crater. The ASTER VNIR imagery improves significantly upon the rough maps of Holdgate & Baker (1979) in characterizing the island's morphology. The 500–600 m wide summit crater (presumed to be the small fresh-looking crater mapped by Holdgate & Baker 1979) now comprises a subtle depression within the summit caldera (Fig. 24a), as originally noted by Smellie *et al.* (1998). A breach in the west rim of the caldera appears to have channelled material erupted from the active crater, creating Morrell Point and Cape Flannery, although this is not yet confirmed from geological studies on the ground.

We also note that the shape of the island shown by our satellite images is somewhat different to that in the rough map of Holdgate & Baker (1979) (Fig. 24b). For instance, the coastline east of Mount Larsen is shown in the Holdgate & Baker (1979) map to be convex towards Douglas Strait, whereas the satellite images show this portion of coastline to be concave towards the strait. We assume this difference is due to errors in the Holdgate & Baker (1979) map, and not to morphological changes, because other distortions are obvious (e.g. the area around Beach Point).

South Atlantic Ocean

Bouvet Island

Bouvet Island (Fig. 1) has had reported fumarolic activity around its caldera (LeMasurier & Thomson 1990), but no thermal anomalies were observed in our survey (Fig. 25a).

South Indian Ocean

Marion Island

Marion Island (24 km wide) resides in the south Indian Ocean (Fig. 1) and comprises two coalesced basaltic shield volcanoes (highest is 1230 m a.s.l.) covered with *c.* 150 cinder cones and a smaller number of surtseyan tuff cones (Fig. 25b). The first recorded eruption occurred sometime between February and October 1980, forming two new cinder cones and three lava flows on the south-west side of the island (Smithsonian Institution 1981, Verwoerd *et al.* 1981, LeMasurier & Thomson 1990). The most recent recorded eruption occurred on 24 June 2004, when a field researcher discovered and filmed a minor eruption of "gas and small pieces of scoria (a few cm in diameter)" on the south part of the island, emanating from a small lake in a pre-existing cone. Scoria was later found to have burnt vegetation (Smithsonian Institution 2004c; I. Meiklejohn, personal communication 2006). We interpret this report to reflect a small strombolian eruption, presumably short in duration. No MODVOLC alerts occurred at Marion in the study period, and ASTER imagery shows no indications of eruptive activity. Several 1–2 pixel ASTER TIR anomalies were coincident with small lakes within several cinder cones on the south-east portion of the island, probably

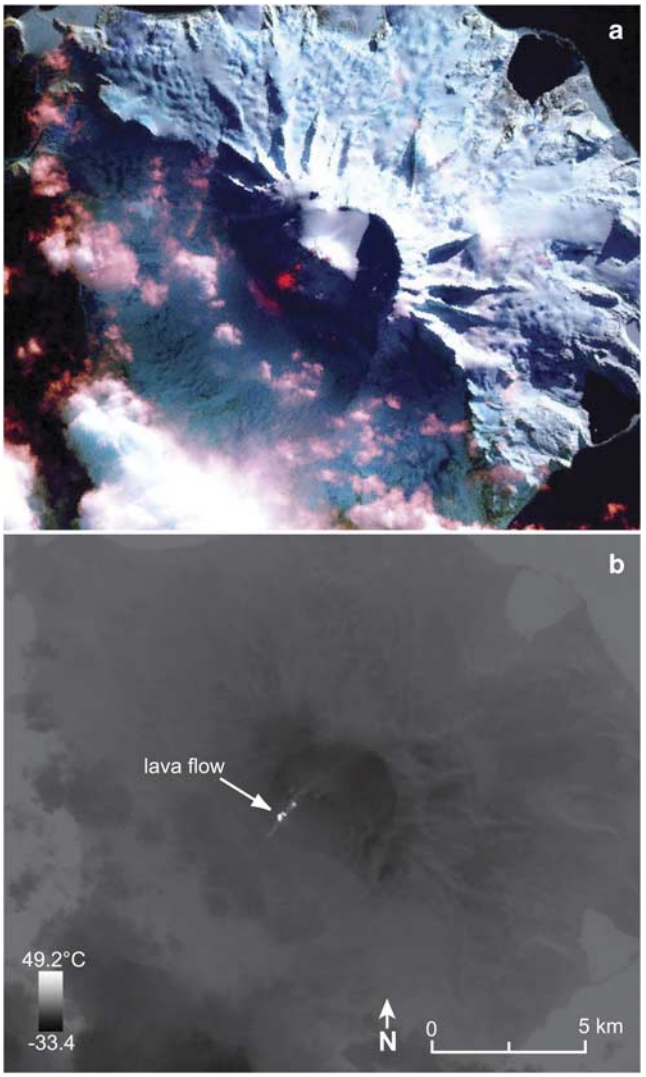

Fig. 26. Big Ben, Heard Island. **a.** Landsat 7 ETM+ (Enhanced Thematic Mapper Plus) composite visible and SWIR (shortwave infrared) image (Bands 7-3-2 RGB) showing a lava flow (bright red) travelling south-west from the summit of Mawson Peak. Image acquired on 7 July 2000, during the first eruptive phase of the study period (2000–01). **b.** Same view and date as above, but showing the Band 6 thermal infrared image, in which the flow can be seen more clearly. Scale values show at-sensor pixel-integrated brightness temperature.

https://doi.org/10.1017/S0954102013000436 Published online by Cambridge University Press

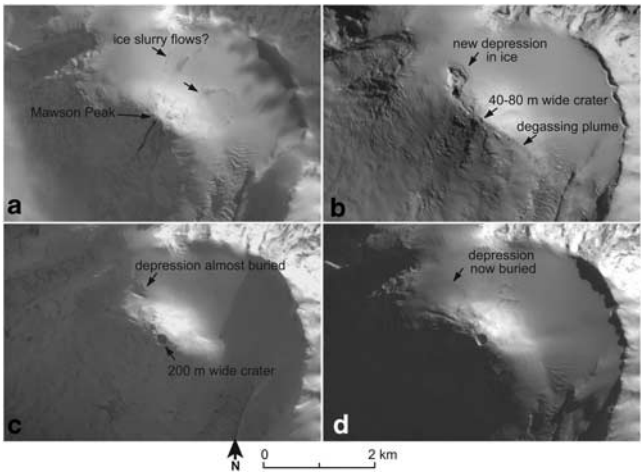

Fig. 27. Changes around Mawson Peak, at the summit of Big Ben on Heard Island. **a.** EO-1 ALI (Earth Observing 1 Advanced Land Imager) Band 1 (panchromatic) image from 28 March 2004. Two wide surface deposits, marked by arrows, may be products of ice-slurry flows. A third feature (dark line), extending south-west of the summit of Mawson Peak, appears to represent a debris flow or narrow lava flow. **b.** EO-1 ALI Band 1 image from 6 December 2007, showing a depression in the ice about 300 x 500 m in size, and about 800 m north-west of the summit crater, that may be due to a lava flow or the opening of a new subordinate vent. The summit crater appears to be 40–80 m wide here. **c.** EO-1 ALI Band 1 image from 4 July 2009, showing that the depression in the ice in part b. is mostly filled with snow and ice. Also, the summit crater had enlarged to *c.* 200 m wide. **d.** EO-1 ALI Band 1 image from 10 September 2010, showing that the depression in the ice is completely buried.

reflecting simply the differing thermal inertia of the water and adjacent ground.

Heard Island (Big Ben)

Heard Island (35 x 20 km) is situated in the southern Indian Ocean, near the Iles Kerguelen (Fig. 1), and is dominated by Big Ben, a large ice-covered basaltic stratocone (Fig. 2). The summit, Mawson Peak (2745 m a.s.l.), has hosted a small lava lake showing episodic activity in recent times (e.g. Smithsonian Institution 1985). Mawson Peak comprises a young cone built within a sector collapse scar (or possibly caldera remnant; LeMasurier & Thomson 1990) directed south-west. Several recent eruptive phases have resulted in lava flows travelling south-west down the ice-covered flanks. There have also been reports of a secondary vent several hundred meters below the summit crater of Mawson Peak (Smithsonian Institution 2000).

MODVOLC alerts indicated that eruptive activity at Heard Island comprised three sustained episodes during our study period (Fig. 4). The first alert period spanned 24 May 2000–2 February 2001 (Smithsonian Institution 2003c). A Landsat ETM+ image acquired on 7 July 2000 shows an active lava flow extending 2 km south-west from the summit of Mawson Peak (Fig. 26). MODVOLC alert pixels extended a significant distance from the summit of Mawson Peak (Fig. 4) only during late November 2000, reaching up to 3 km down the south-west flank (Fig. 4; Smithsonian Institution 2003c), reflecting the apparent emplacement of a second flow. It is noteworthy that MODVOLC did not register the 7 July 2000 effusive event; no alerts occurred between 10 June and 30 July, suggesting that the Landsat image may have been a fortuitous cloud-free acquisition during an otherwise cloudy period.

After the first eruptive episode, quiescence was maintained for more than two years. An EO-1 ALI image from July 2002 shows a snow-covered vent area and a small, but faint SWIR anomaly at the summit, which may reflect high-temperature fumaroles. MODVOLC alerts returned on 9 June 2003, signalling the start of the second eruption, and alerts were sustained until 14 June 2004 (Smithsonian Institution 2004a). No alert pixels were present a significant distance from the summit, and temporal coverage of alerts was more continuous in this phase, suggesting that activity was largely limited to the summit vent and any flows which did extend outside the vent were relatively short. ASTER images acquired during this phase confirm this, with small TIR and night-time SWIR anomalies for the most part confined to the summit region. In three scenes during this phase (17 August 2003, 12 November 2003, 15 May 2004), elongate TIR anomalies extended a maximum of 400–600 m, which may reflect small flows from the summit crater. An EO-1 ALI image from 28 March 2004, shows two wide (270–700 m) and long (1.2–1.6 km) flow-like features extending north of the summit vent (Fig. 27a). These do not appear to be lava flows, as they have not cut into the deep ice cover, and may be ice-slurry flows mobilized by hot material at the vent, perhaps similar to the ice-slurry flows at Redoubt (Pierson & Janda 1994) and Ruapehu (Lube *et al*. 2009).

The second eruption, which ended around June 2004, was followed by almost two years of inactivity, and an EO-1 ALI image from November 2004 shows the northern ice-slurry flows already buried by snow, and the summit covered by rime ice. The third eruptive episode began in March 2006, with MODVOLC alerts indicating eruptive activity for the next two years, between 11 March 2006 and 2 March 2008. Similar to the second eruption, there was no evidence of very long lava flows, but short flows were apparently erupted. EO-1 ALI images in January and March 2007 appear to show short ($<$ 300 m long) flows extending from the summit vent. A Google Earth image from May 2007 shows a new north-west-trending trench starting from near the summit and leading to a 300 m wide crevasse-bounded depression in the ice 800 m north-west of the summit vent. A EO-1 ALI image in December 2007 shows that this depression had enlarged to about 500 m long (Fig. 27b). It is not clear what caused the trench and

https://doi.org/10.1017/S0954102013000436 Published online by Cambridge University Press

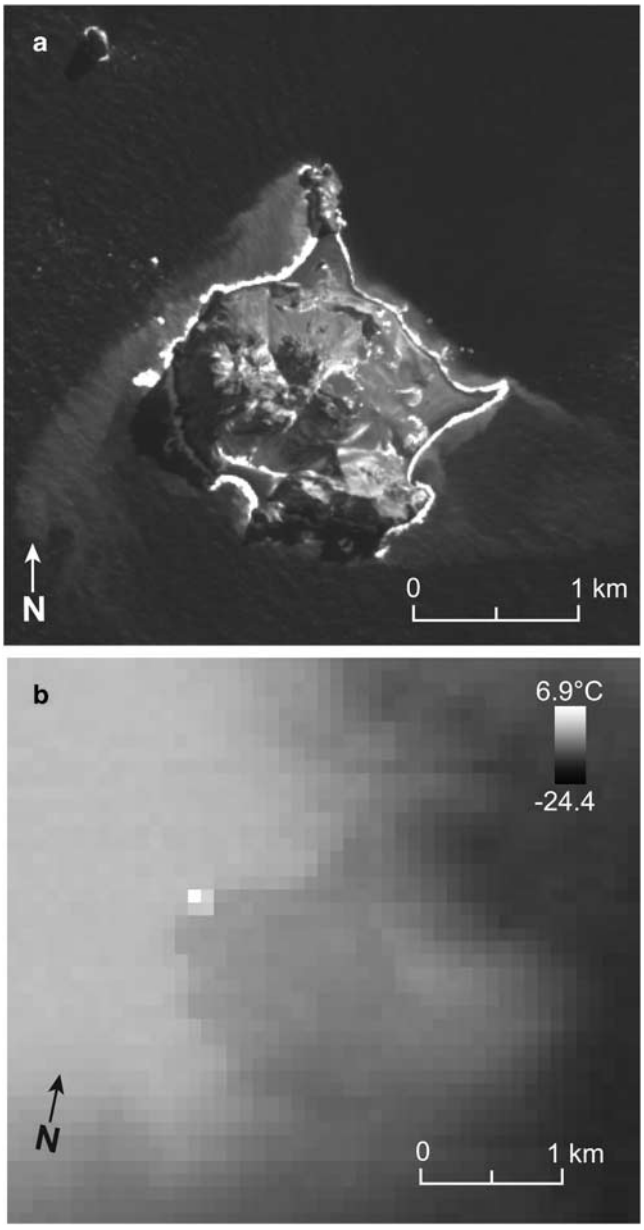

Fig. 28. McDonald Island. **a.** EO-1 ALI (Earth Observing 1 Advanced Land Imager) Band 1 (panchromatic) image from 26 March 2011, showing the structure of McDonald Island, which is composed of overlapping domes and spines, much of which has been erupted in the last 20 years. **b.** ASTER (Advanced Spaceborne Thermal Emission and Reflection Radiometer) Band 14 (thermal infrared) image from 12 July 2005, showing apparent eruptive activity in the north-west portion of the island. Scale values show at-sensor pixel-integrated brightness temperature.

depression, but it may have resulted from a narrow lava flow erupted near the summit that ponded lower down where it slowed due to encountering thick ice in the area of depression. Alternatively, it may represent the opening of a subordinate vent north-west of the main summit vent. The third eruption ended in March 2008, and ASTER images collected over the subsequent two years showed no signs of eruptive activity (Smithsonian Institution 2010b).

MODVOLC alerts show three distinct eruptive episodes with apparently no sporadic activity occurring between eruptions (Fig. 4). Most radiant heat flux values were between 10 and 60 MW, but one approached 200 MW on 28 November 2003. A Quickbird browse image from November 27 shows a short fresh-looking flow extending north of the summit, suggesting high lava levels in the summit crater. The overall mean radiant heat output of the study period was 23 MW, similar to that of Mount Belinda. The MODVOLC data also show that the third eruptive episode appeared to "sputter out" (unlike the first two episodes that ended relatively abruptly) with gaps in alerts up to several months before the final end in March 2008. We suspect this reflects actual activity levels and not simply changes in cloud cover.

EO-1 ALI and ASTER images show that the summit crater enlarged significantly during the study period. Throughout the first two eruptions and their subsequent repose intervals, the summit vent was small, and less than 100 m wide. More precisely, a Google Earth image in May 2007 shows the summit crater clearly at 40 m wide. An EO-1 ALI image, which is much lower resolution than the Google Earth image, from December 2007 shows a dark region around the summit crater that is 80 m wide (Fig. 27b). This may be the actual crater dimension, or shadow making the crater appear larger than it actually was (i.e. it may have been between 40 and 80 m wide at that time). At some time in 2008 or early 2009 (bracketed by images on 23 March 2008 and 3 February 2009) the summit crater widened to 200 m (Fig. 27c & d). As no evidence of explosive activity was observed, we speculate that this enlargement was due to magma withdrawal after the end of the third eruption removing support from the upper conduit, triggering collapse. This is not the first observation of vent geometry changes at the summit of Mawson Peak. A climbing expedition to the summit in 1983 noted no summit vent, but an expedition in 1986–87 found a 50 m diameter crater with a lava lake at 50–70 m depth (LeMasurier & Thomson 1990). That crater appearance may have been related to an eruption in early 1985, when a 7 km long lava flow was observed (LeMasurier & Thomson 1990).

Unlike the eruptive activity at Mount Belinda, the activity at Heard Island was entirely effusive and there is no evidence for any low-level explosive activity. No ash cover was observed on the snow in any of the images, and the small plumes emanating from the summit vent were all white in colour, indicative of passive degassing.

McDonald Island

McDonald Island is a single small island (presently 2.4 km x 2.1 km), *c.* 45 km west of Heard Island (Fig. 2b), composed of overlapping phonolite domes and lava flows

https://doi.org/10.1017/S0954102013000436 Published online by Cambridge University Press

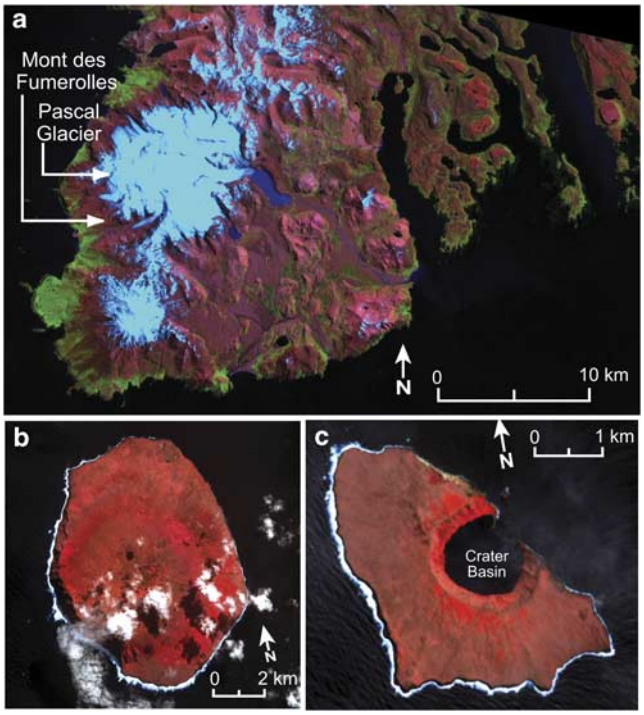

Fig. 29. a. Péninsule Rallier du Baty in the south-west portion of the Iles Kerguelen. Landsat 7 ETM+ (Enhanced Thematic Mapper Plus) Bands 7-4-2 RGB, from 27 November 2001. Fumarolic activity appears to persist in the aptly named Mont des Fumerolles region. **b.** ASTER (Advanced Spaceborne Thermal Emission and Reflection Radiometer) VNIR (visible/near infrared) (Bands 3-2-1 RGB) of Amsterdam Island on 12 March 2007. **c.** ASTER VNIR (Bands 3-2-1 RGB) image of St Paul Island from 10 November 2000.

(Fig. 28a) built upon the Kerguelen submarine plateau (LeMasurier & Thomson 1990). Shuttle Radar Topography Mission elevation data from February 2000 indicate a peak elevation of 275 m. There was no known historic activity until 1997, when steam and possible new deposits were noted on the northern end of the island (Stephenson *et al*. 2005). Before recent activity ensued, the McDonald Islands comprised three primary islands. A Landsat ETM+ image from 2001, analysed by the Australian Antarctic Division, showed that the total island area had approximately doubled in size, since photography and a landing were made in 1980, connecting the three islands into a single landmass (Smithsonian Institution 2002). Stephenson *et al*. (2005) used high-resolution imagery and photos from a ship to thoroughly document the recent changes to the island, which include a substantial new complex of domes, spines and viscous flows.

The sole MODVOLC alert on McDonald Island occurred on 14 November 2004 (Smithsonian Institution 2004b), indicating renewed, but apparently brief, activity during our study period. The total radiant heat flux of this single alert pixel was 10 MW, lower than the average heat output of the other erupting volcanoes in this study. ASTER imagery includes only a half-dozen cloud-free scenes, with several showing a thermal anomaly on the shoreline in the north-western portion of the island. The July 2005 night-time scene (Fig. 28b) features both a SWIR and TIR anomaly (Smithsonian Institution 2005c). This confirmation of activity in July 2005 led to a press release by the Australia Antarctic Division which garnered a modest amount of attention from news media. Comparison of an EO-1 ALI image from 26 March 2011 (Fig. 28a) with the November 2001 Landsat indicates only minor, if any, expansion (< 100 m) to the coastline in the north-west portion of the island, indicating that the total effusive volume erupted during the study period was modest. Most likely, the activity comprised the brief eruption of a small spine or dome.

Iles Kerguelen

Fumarolic activity has been studied on the Rallier du Baty Peninsula (Ballestracci & Nougier 1984, LeMasurier & Thomson 1990). Cloud-free ASTER and Landsat (Fig. 29a) images show no obvious thermal anomalies. A winter high-resolution image on Google Earth, from August 2006, shows an anomalous snow-free area with possible steaming at 49.625°S, 68.809°E (WGS84 datum) which corresponds with the main fumarolic area, at Mont des Fumerolles, as marked by zone 4 in Ballestracci & Nougier (1984) suggesting that these fumaroles remained active in the study period. Snow-free areas, and possible steam plumes, were also apparent in this image at Pascal Glacier, in zone 3 of Ballestracci & Nougier (1984).

St Paul and Amsterdam islands

St Paul is a small (3 x 5 km; 268 m a.s.l.) tholeiitic basalt island in the south Indian Ocean (Fig. 1) hosting an 1800 m diameter central crater that is breached to the north-east (Fig. 29c). Gaseous emissions and fresh ash were observed on a cinder cone on the south-west flank in 1793, suggesting a recent eruption (LeMasurier & Thomson 1990). Fumarolic activity has been noted numerous times on the crater rim as well as along the crater shoreline. No obvious thermal anomalies were observed in ASTER TIR imagery. Amsterdam Island (10 x 7 km, 881 m a.s.l.) is a larger neighbour to St Paul, with an eruption sometime in the last 100 years inferred from a lava flow with a young appearance (LeMasurier & Thomson 1990). ASTER images show no indications of activity in our study period (Fig. 29b).

Summary of 2000–10 activity

Eruptive activity

Eruptive activity, as indicated by MODVOLC alerts (Fig. 4), was observed at five volcanoes in this 2000–10 survey: 1) Mount Erebus, Antarctica, 2) Mount Belinda, Montagu Island, South Sandwich Islands, 3) Mount

https://doi.org/10.1017/S0954102013000436 Published online by Cambridge University Press

Michael, Saunders Island, South Sandwich Islands, 4) Big Ben, Heard Island, and 5) McDonald Island, also in the Heard Island group. All of these were low-level, predominantly effusive eruptions. All but one involved lava active within open craters. Only the eruption of Mount Belinda produced notable tephra.

Mount Erebus activity has been continuous throughout 2000–10 and confined to the relatively small lava lake in the summit crater (Fig. 5a). Mount Belinda (Montagu Island), in the South Sandwich Islands, began its first recorded eruption in September–October 2001 with low-level explosive activity and a continuous degassing plume punctuated by the effusion of several lava flows (Fig. 16). The eruption also built an 800 m wide delta on the north coast of the island (Figs 17 & 20a). The eruption ended in late 2007, totalling six years of continuous low-level eruptive activity. Mount Michael showed sporadic MODVOLC thermal alerts and at least one instance of lava observed filling its summit crater (Fig. 14), indicating that eruptive activity in its crater is more sporadic than occurs at Mount Erebus. However, like Mount Erebus, the Mount Michael crater is thought to host a semi-persistent fluctuating lava lake (Lachlan-Cope *et al*. 2001), although there might be some years, or substantial parts of years, when the lake is absent (as is perhaps the case now). We also document a new active vent south-east of the main crater on Mount Michael (Fig. 14). Big Ben, on Heard Island, experienced three eruptions (Fig. 4) in the study period: May 2000–February 2001, June 2003–July 2004, and March 2006–March 2008. The first episode saw the emplacement of at least two lava flows (each 2–3 km long) down the south-western flank (Fig. 26) while the latter two episodes appeared to have had most activity within or near the summit vent (Fig. 27). The third eruption was associated with dramatic summit crater enlargement, from 40–200 m diameter. McDonald Island, adjacent to Heard Island, experienced further eruptive activity - presumably low-level effusion in the form of small spines and domes - which appeared to be centred on the north to north-western sectors of the island (Fig. 28). McDonald Island produced only a single MODVOLC alert, in November 2004.

Fumarolic activity

ASTER thermal anomalies registering non-eruptive episodes were interpreted to indicate fumarolic activity, sufficient in intensity and/or spatial extent to be detected by the 90 m TIR pixels. This level of fumarolic activity was observed at two locations on Deception Island (Fig. 9), consistent with previously reported locations, although many other reported fumarolic areas on the island were not detected with the satellite data. The Bellingshausen (Fig. 23) and Candlemas (Fig. 13) fumarole locations were also consistent with previous reports. Steaming has been reported at Zavodovski Island, and this study suggests that thermal activity is most intense on the west wall of the crater (Fig. 11b). Alternatively, the outer flanks may be less obscured by the persistent steaming within the crater. Bristol Island has experienced several eruptions in recorded history, and the persistent snow-free zone at the summit of Mount Sourabaya (Fig. 22b) attests to its continued thermal activity, while providing possible evidence that Mount Sourabaya may be the source of observed eruptions in 1935 and 1956. Thermal anomalies are present at Mount Sourabaya as well as the small crater to its east (Fig. 22c). Apparent elevated temperatures in thermal imagery over Leskov Island (Fig. 12c) were consistent with the location of known fumaroles along the summit ridge, but the island is so small that it is difficult to discount solar heating. Small thermal anomalies were observed at Mount Rittmann but it was difficult to tell with certainty if these were associated with the fumarolic activity reported there.

No detectable activity

Several volcanoes which have had reported historic activity showed no detectable signs of activity in our survey. Mount Hodson (Fig. 12a), on Visokoi Island, was observed in 1830 as "a burning mountain with smoke issuing from it in several places" (LeMasurier & Thomson 1990). ASTER imagery shows no indication of thermal activity. Both Mount Siple (Fig. 7c) and Webber Nunatak (Fig. 8b) had reported eruption plumes in low spatial-resolution satellite imagery. Doubt about the Mount Siple report was expressed after a later overflight and the Webber Nunatak report also remains uncertain. Our survey shows no indication of activity in the study period, nor any conspicuous evidence of recent activity at these volcanoes. The reported historic activity at Seal Nunataks is conflicting. Whilst the observations made in 1893 are relatively convincing and suggest vigorous steam emission, at least, and some steam was described as black and thick suggesting it might have had an ash content, no explosions were mentioned and there are no obvious primary volcanic landforms for such a recent event. Our survey also shows that no eruptive activity occurred in the study period and no large areas of actively warm ground seem to be present (Fig. 8a). Finally, no indications of volcanic activity were observed at Bouvet Island (Fig. 25a) or Buckle Island (Fig. 6b). Although fumarolic activity has been noted on Mount Melbourne, Mount Berlin and Mount Kauffman, and Bridgeman Island, St Paul Island and Iles Kerguelen, any fumarolic activity in 2000–10 was not sufficient in intensity or extent to be detected with confidence in the ASTER TIR imagery. Fumarolic activity at Mount Melbourne still existed in January 2006 (JLS, personal observation).

Undetected activity

A minor eruption observed on Marion Island in June 2004 was detected neither in MODVOLC nor ASTER

https://doi.org/10.1017/S0954102013000436 Published online by Cambridge University Press

data (Fig. 25b). The eruption was described as a small strombolian event occurring from a pre-existing crater; it was not a sustained cone-building episode. Wright *et al*. (2004) discussed how the regular strombolian events at Stromboli Volcano, Italy, very rarely trigger the MODVOLC system, presumably due to the transience of the explosions and the modest amounts of lava produced during typical strombolian behaviour (Chouet *et al*. 1974). It is important to note that persistent cloud-cover at other volcanoes in the region means that some low-level activity might have been missed in this survey.

Discussion and conclusions

Previous studies (Dean *et al*. 2004, Patrick *et al*. 2005, Bailey *et al*. 2010, Webley *et al*. 2012) have used a diverse assortment of imagery to chronicle remote eruptions. In this study, we focus our efforts on two datasets that provide the greatest amount of information for their cost and availability: MODVOLC-MODIS and ASTER. Carn & Oppenheimer (2000) followed a similar principle in limiting their data to AVHRR and SPOT (Système Pour l'Observation de la Terre) browse imagery, and Rothery *et al*. (2005) used MODVOLC data exclusively for a regional analysis of volcanic activity in Indonesia. MODVOLC allows daily tracking of activity to garner a rough sense of eruptive intensity, while ASTER data provide a high spatial resolution snapshot of activity, albeit with infrequence. MODVOLC data can be examined online in just a few minutes; ASTER imagery can be downloaded within a few days of their acquisition, and given their infrequence do not constitute a great time demand. As mentioned, MODVOLC data are free and ASTER scenes can be obtained free of charge in some cases. These time- and cost-efficiencies are practical for observatories that may not have a designated remote sensing division.

One purpose of this study was to establish with the ASTER imagery whether the effects of any recent eruptive activity (prior to 2000) could be observed. LeMasurier & Thomson (1990) noted how the effects of all but the largest eruptions, however, can be rapidly obscured in the Antarctic and sub-Antarctic environment. For instance, our study showed that the 200 m wide and 60 m deep crater observed in 1962, on the western side of Bristol Island, was completely buried by snow and ice in 2000–10 images. Also, on Heard Island a deep depression that formed in the ice north-west of the summit in 2007 (Fig. 27b) was buried by 2010 (Fig. 27d). Dean *et al*. (2002) observed that the 1.5 km wide by 500 m deep crater formed during the 1978 eruption of Westdahl Volcano, Alaska, was completely buried by snow and ice by 1992. Morphological evidence for past minor/moderate eruptive activity therefore appears to have a short observable lifespan in polar environments (see also Gudmundsson *et al*. 2002).

Wright *et al*. (2004) described how MODVOLC was designed so that its detection threshold is set high to avoid false alerts, resulting in low-level eruptive activity and passive emissions (such as fumaroles) eluding detection. For instance, the sporadic alerts at Mount Michael (Fig. 4) suggest that lava activity fluctuates in intensity, of which only the most vigorous instances are detected, or else the lake subsides (drains) periodically whilst being broadly a persistent feature (Lachlan-Cope *et al*. 2001). The latter seems to be supported by significant, although muted, levels of activity that appear to be maintained at Mount Michael in the periods between MODVOLC alerts, as ASTER images show steam plumes and saturated SWIR pixels in the summit crater during these intervening phases. On the other hand, during the interval between the 2000–01 and 2003–04 sustained eruptive phases at Heard Island, when no MODVOLC alerts were observed, ASTER imagery shows that no significant activity was in place. No ASTER SWIR anomalies were observed, and only extremely faint TIR anomalies were observed in the intervening period. Thus, Mount Michael appears to exhibit persistent, although generally low-level, activity while Heard Island exhibits more episodic behaviour.

The known fumarolic activity at mounts Melbourne, Berlin and Erebus, and the lack of associated thermal anomalies in ASTER, show clearly that ASTER is not capable of detecting some fumarolic activity. At Candlemas and Bellingshausen islands, fumarolic activity is conspicuous in ASTER TIR imagery due to its wide distribution and the resulting lack of snow cover. At mounts Melbourne, Berlin and Erebus, many of the fumaroles create ice towers (LeMasurier & Thomson 1990), which visually and thermally obscure any underlying hot surfaces. Even in cases where fumarolic activity is exposed on bare rock, two issues limit ASTER detection. First, on a snow and ice-covered volcano the fumarolically-heated areas of bare rock may not stand out appreciably from nearby rock which is bare due to topography or solar heating. Second, in the absence of snow and ice-cover the area of fumarolically-heated ground must be sufficiently large to create a conspicuous signal in a 90 x 90 m pixel. For example, despite high temperatures (*c.* 90°C) measured in fissures on bare rock high on Deception Island, the temperatures fall off rapidly and are undetectable. Thus, fumarolic activity is often scattered, with appreciably hot surfaces comprising a minute total surface area. An additional factor may be local conditions. Using Deception Island again, despite the fumarolic areas being individually quite large (often well above pixel dimensions), most are located between high and low tide marks and are covered and therefore obscured during high tides.

This study could be improved substantially with the acquisition of full-resolution IKONOS, QuickBird, GeoEye and WorldView imagery, which have pixel sizes ranging from 50 cm to 4 m. These data would be particularly helpful in: a) tracking the episodes of effusion at Mount Belinda, b) examining the interior of the summit crater at Mount Michael, c) investigating the possibility of multiple vents

https://doi.org/10.1017/S0954102013000436 Published online by Cambridge University Press

on Heard Island, and d) generally relating surface morphologies and structures to observed eruptive and fumarolic activity. While these sensors lack thermal infrared bands, the higher spatial resolution would be helpful in identifying smaller anomalous snow-free areas suggestive of fumarolic activity which could not be discerned with the 15 m ASTER VNIR data. In some cases, the near-infrared bands on these commercial sensors could help detect active lava. Atmospheric remote sensing data were not analysed in this study but could provide improved understanding of the volcanoes in this region. Future work could involve focusing on eruptions identified in this study, such as those at Mount Belinda, Mount Michael and Heard Island, to better understand the nature and rates of volcanic gas emission. Sulfur dioxide retrievals can be performed with ASTER and MODIS data, and detection of ash plumes is possible with these data as well (Bailey *et al*. 2010, Webley *et al*. 2012). Gassó (2008) showed that the weak volcanic activity at Mount Belinda and Mount Michael impacted the nature of surrounding meteorological clouds, reducing cloud particle size and making conspicuous cloud tracks extending out from the volcanoes. This method may be useful for identifying future activity in the region. Synthetic aperture radar (SAR) imagery could also be very useful in the region, given its ability to penetrate cloud cover.

In conclusion, this study uses satellite imagery to provide a geographically comprehensive inventory of the 2000–10 volcanic activity in Antarctica and the southern oceans, a region where the historic record has been greatly limited due to inaccessibility. Coupled analysis of MODVOLC and ASTER, like that used in this study, should enable improved tracking of volcanism throughout the region in the future.

Acknowledgements

The authors primarily wish to thank the Smithsonian Institution staff overseeing the Global Volcanism Program, particularly R. Wunderman and L. Siebert, for their input and assistance on this project. We also benefited from valuable correspondence with A. Tupper (Darwin VAAC), M. Stoddart (Australian Antarctic Division), and personnel from the Toulouse VAAC regarding Heard and McDonald islands. Photographs were kindly shared by I. Hunter and Capt. D. Hall of the South African Weather Service from their January 2006 visit to Thule and Montagu islands. HVO volunteer Tristan McDonald devoted much time to downloading ASTER images. Several Landsat scenes were downloaded from the University of Maryland Global Land Cover Facility. The IKONOS image over Montagu Island was made public by J. Garvin (NASA). We thank A. Harris for general advice, R. Wright for advice regarding MODVOLC, and H. Garbeil for assistance with ASTER data. Dr Patrick performed much of the work on this paper while at University of Hawaii Manoa and Michigan Technological University. Reviews by Rick Wessels, Greg Vaughan, Simon Carn and Peter Webley are greatly appreciated.

References

Aster, R., McIntosh, W., Kyle, P., Esser, R., Bartel, B., Dunbar, N., Johns, B., Johnson, J., Karstens, R., Kurnik, C., McGowan, M., McNamara, S., Meertens, C., Pauly, B., Richmond, M. & Ruiz, M. 2004. New instrumentation delivers multidisciplinary real-time data from Mount Erebus, Antarctica. *EOS Transactions*, **85**, 100–101.

Bailey, J.E., Dean, K.G., Dehn, J. & Webley, P.W. 2010. Integrated satellite observations of the 2006 eruption of Augustine Volcano. *In* Power, J.A., Coombs, M.L. & Freymueller, J.T., *eds.* The 2006 eruption of Augustine Volcano, Alaska. *US Geological Survey Professional Paper*, **1769**, 481–506.

Ballestracci, R. & Nougier, J. 1984. Detection by infrared thermography and modeling of an icecapped geothermal system in Kerguelen Archipelago. *Journal of Volcanology and Geothermal Research*, **20**, 85–99.

Bargagli, R., Broady, P.A. & Walton, D.W.H. 1996. Preliminary investigation of the thermal biosystem of Mount Rittmann fumaroles (northern Victoria Land, Antarctica). *Antarctic Science*, **8**, 121–126.

Calder, E.S., Harris, A.J.L., Peña, P., Pilger, E., Flynn, L.P., Fuentealba, G. & Moreno, H. 2004. Combined thermal and seismic analysis of the Villarrica volcano lava lake, Chile. *Revista Geológica de Chile*, **31**, 259–272.

Carn, S.A. & Oppenheimer, C. 2000. Remote monitoring of Indonesian volcanoes using satellite data from the internet. *International Journal of Remote Sensing*, **21**, 873–910.

Chouet, B., Hamisevicz, N. & McGetchin, T.R. 1974. Photoballistics of volcanic jet activity at Stromboli, Italy. *Journal of Geophysical Research*, **79**, 4961–4976.

Convey, P. & Smith, R.I.L. 2006. Responses of terrestrial Antarctic ecosystems to climate change. *Plant Ecology*, **182**, 1–10.

Csatho, B., Schenk, T., Kyle, P., Wilson, T. & Krabill, W.B. 2008. Airborne laser swath mapping of the summit of Erebus Volcano, Antarctica: applications to geological mapping of a volcano. *Journal of Volcanology and Geothermal Research*, **177**, 531–548.

Davies, A.G., Calkins, J., Scharenbroich, L., Vaughan, R.G., Wright, R., Kyle, P., Castano, R., Chien, S. & Tran, D. 2008. Multi-instrument remote and *in situ* observations of the Erebus volcano (Antarctica) lava lake in 2005: a comparison with the Pele lava lake on the Jovian moon Io. *Journal of Volcanology and Geothermal Research*, **177**, 705–724.

Dean, K.G., Engle, K., Groves, J., Dehn, J. & Partington, K. 2002. Analysis of surface processes using SAR data: Westdahl Volcano, Alaska. *International Journal of Remote Sensing*, **23**, 4529–4550.

Dean, K.G., Dehn, J., Papp, K.R., Smith, S., Izbekov, P., Peterson, R., Kearney, C. & Steffke, A. 2004. Integrated satellite observations of the 2001 eruption of Mount Cleveland, Alaska. *Journal of Volcanology and Geothermal Research*, **135**, 51–73.

Dehn, J., Dean, K.G., Engle, K. & Izbekov, P. 2002. Thermal precursors in satellite images of the 1999 eruption of Shishaldin volcano. *Bulletin of Volcanology*, **64**, 525–534.

Edwards, B., Magnússon, E., Thordarson, T., Gudmundsson, M.T., Höskuldsson, A., Oddson, B. & Haklar, J. 2012. Interactions between lava and snow/ice during the 2010 Fimmvörrduháls eruption, south-central Iceland. *Journal of Geophysical Research*, 10.1029/2011JB008985.

Gassó, S. 2008. Satellite observations of the impact of weak volcanic activity on marine clouds. *Journal of Geophysical Research*, 10.1029/2007JD009106.

Gerlach, T. 2011. Volcanic versus anthropogenic carbon dioxide. *Eos Transactions*, **92**, 201–208.

Gudmundsson, M.T., Pálsson, F., Björnsson, H. & Högnadóttir, Th. 2002. The hyaloclastite ridge formed in the subglacial 1996 eruption in Gjálp, Vatnajökull, Iceland: present-day shape and future preservation. *In* Smellie, J.L. & Chapman, M.G., *eds. Volcano-ice interaction on Earth and Mars. Special Publication of the Geological Society of London*, No. 202, 319–335.

Harris, A.J.L., Wright, R. & Flynn, L.P. 1999. Remote monitoring of Mount Erebus volcano, Antarctica, using Polar Orbiters: progress and prospects. *International Journal of Remote Sensing*, **20**, 3051–3071.

Harris, A.J.L., Butterworth, A.L., Carlton, R.W., Downey, I., Miller, P., Navarro, P. & Rothery, D.A. 1997. Low-cost volcano surveillance from space: case studies from Etna, Krafla, Cerro Negro, Fogo, Lascar and Erebus. *Bulletin of Volcanology*, **59**, 49–64.

Holdgate, M.W. & Baker, P.E. 1979. The South Sandwich Islands: I. General description. *British Antarctic Survey Scientific Reports*, **91**, 76 pp.

Ibáñez, J.M., Carmona, E., Almendros, J., Saccorotti, G., Del Pezzo, E., Abril, M. & Ortiz, R. 2003. The 1998–1999 seismic series at Deception Island volcano, Antarctica. *Journal of Volcanology and Geothermal Research*, **128**, 65–88.

Kaufman, Y.J., Justice, C.O., Flynn, L.P., Kendall, J.D., Prins, E.M., Giglio, L., Ward, D.E., Menzel, W.P. & Setzer, A.W. 1998. Potential global fire monitoring from EOS-MODIS. *Journal of Geophysical Research*, **103**, 32 215–32 238.

Kyle, P.R. *ed.* 1994. Volcanological and environmental studies of Mount Erebus, Antarctica. *Antarctic Research Series*, **66**, 162 pp.

Lachlan-Cope, T., Smellie, J.L. & Ladkin, R. 2001. Discovery of a recurrent lava lake on Saunders Island (South Sandwich Islands) using AVHRR imagery. *Journal of Volcanology and Geothermal Research*, **112**, 105–116.

Leat, P.T., Smellie, J.L., Millar, I.L. & Larter, R.D. 2003. Magmatism in the South Sandwich arc. *In* Larter, R.D. & Leat, P.T., *eds. Intra-oceanic subduction systems: tectonic and magmatic processes. Special Publication of the Geological Society of London*, No. 219, 285–313.

Leat, P.T., Tate, A.J., Tappin, D.R., Day, S.J. & Owen, M.J. 2010. Growth and mass wasting of volcanic centers in the northern South Sandwich arc, South Atlantic, revealed by new multibeam mapping. *Marine Geology*, **275**, 110–126.

LeMasurier, W.E. & Thomson, J.W. *eds.* 1990. Volcanoes of the Antarctic Plate and Southern Oceans. *Antarctic Research Series*, **48**, 487 pp.

Lescinsky, D.T. & Fink, J.H. 2000. Lava and ice interaction at stratovolcanoes: use of characteristic features to determine past glacial extents and future volcanic hazards. *Journal of Geophysical Research*, **105**, 23 711–23 726.

Lube, G., Cronin, S.J. & Procter, J.N. 2009. Explaining the extreme mobility of volcanic ice-slurry flows, Ruapehu volcano, New Zealand. *Geology*, **37**, 15–18.

Major, J.J. & Newhall, C.G. 1989. Snow and ice perturbation during historical volcanic eruptions and the formation of lahards and floods. *Bulletin of Volcanology*, **52**, 1–27.

Masuoka, E., Fleig, A., Wolfe, R.E. & Patt, F. 1998. Key characteristics of MODIS data products. *IEEE Transactions on Geoscience and Remote Sensing*, **26**, 1313–1323.

Oppenheimer, C. & Kyle, P.R. 2008. Probing the magma plumbing of Erebus volcano, Antarctica, by open-path FTIR spectroscopy of gas emissions. *Journal of Volcanology and Geothermal Research*, **177**, 743–754.

Patrick, M., Smellie, J.L., Harris, A.J.L., Wright, R., Dean, K., Izbekov, P., Garbeil, H. & Pilger, E. 2005. First recorded eruption of Mount Belinda volcano (Montagu Island), South Sandwich Islands. *Bulletin of Volcanology*, **67**, 415–422.

Pieri, D. & Abrams, M. 2004. ASTER watches the world's volcanoes: a new paradigm for volcanological observations from orbit. *Journal of Volcanology and Geothermal Research*, **135**, 13–28.

Pierson, T.C. & Janda, R.J. 1994. Volcanic mixed avalanches: a distinct eruption-triggered mass-flow process at snow-clad volcanoes. *Geological Society of America Bulletin*, **106**, 1351–1358.

Robock, A. 2000. Volcanic eruptions and climate. *Reviews of Geophysics*, **38**, 191–219.

Rothery, D.A. & Oppenheimer, C. 1994. Monitoring Mount Erebus by satellite remote sensing. *Antarctic Research Series*, **66**, 51–56.

Rothery, D.A., Coppola, D. & Saunders, C. 2005. Analysis of volcanic activity patterns using MODIS thermal alerts. *Bulletin of Volcanology*, **67**, 539–556.

Rothery, D.A., Francis, P.W. & Wood, C.A. 1988. Volcano monitoring using short wavelength infrared data from satellites. *Journal of Geophysical Research*, **93**, 7993–8008.

Rowe, C.A., Aster, R.C., Kyle, P.R., Dibble, R.R. & Schlue, J.W. 2000. Seismic and acoustic observations at Mount Erebus volcano, Ross Island, Antarctica, 1994–1998. *Journal of Volcanology and Geothermal Research*, **101**, 105–128.

Siebert, L., Simkin, T. & Kimberly, P. 2010. *Volcanoes of the world*, 3rd ed. Berkeley, CA: University of California Press, 568 pp.

Smellie, J.L. 1999. The upper Cenozoic tephra record in the south polar region: a review. *Global and Planetary Change*, **21**, 51–70.

Smellie, J.L. & Hole, M.J. 1997. Products and processes in Pliocene–Recent, subaqueous to emergent volcanism in the Antarctic Peninsula: examples of englacial Surtseyan volcano construction. *Bulletin of Volcanology*, **58**, 628–646.

Smellie, J.L. & Skilling, I.P. 1994. Products of subglacial volcanic eruptions under different ice thicknesses: two examples from Antarctica. *Sedimentary Geology*, **91**, 115–129.

Smellie, J.L., Morris, P., Leat, P.T., Turner, D.B. & Houghton, D. 1998. Submarine caldera and other volcanic observations in Southern Thule, South Sandwich Islands. *Antarctic Science*, **10**, 171–172.

Smellie, J.L. & López-Martínez, J. *et al. eds.* 2002. *Geology and geomorphology of Deception Island. BAS GEOMAP Series*, Sheets 6-A and 6-B, 1:25 000, Cambridge: British Antarctic Survey, 78 pp.

Smithsonian Institution. 1981. Marion Island. *Scientific Event Alert Network Bulletin*, **6**, 1.

Smithsonian Institution. 1985. Heard Island. *Scientific Event Alert Network Bulletin*, **10**, 2.

Smithsonian Institution. 1988a. Siple Island. *Scientific Event Alert Network Bulletin*, **13**, 9.

Smithsonian Institution. 1988b. Siple Island. *Scientific Event Alert Network Bulletin*, **13**, 12.

Smithsonian Institution. 2000. Heard Island. *Bulletin of the Global Volcanism Network*, **25**, 11.

Smithsonian Institution. 2002. McDonald Island. *Bulletin of the Global Volcanism Network*, **27**, 12.

Smithsonian Institution. 2003a. Deception Island. *Bulletin of the Global Volcanism Network*, **28**, 2.

Smithsonian Institution. 2003b. Montagu Island. *Bulletin of the Global Volcanism Network*, **28**, 2.

Smithsonian Institution. 2003c. Heard Island. *Bulletin of the Global Volcanism Network*, **28**, 1.

Smithsonian Institution. 2004a. Heard Island. *Bulletin of the Global Volcanism Network*, **29**, 12.

Smithsonian Institution. 2004b. McDonald Island. *Bulletin of the Global Volcanism Network*, **29**, 12.

Smithsonian Institution. 2004c. Marion Island. *Bulletin of the Global Volcanism Network*, **30**, 2.

Smithsonian Institution. 2005a. Montagu Island. *Bulletin of the Global Volcanism Network*, **30**, 9.

Smithsonian Institution. 2005b. Montagu Island. *Bulletin of the Global Volcanism Network*, **30**, 11.

Smithsonian Institution. 2005c. McDonald Island. *Bulletin of the Global Volcanism Network*, **30**, 6.

Smithsonian Institution. 2006a. Mount Michael. *Bulletin of the Global Volcanism Network*, **31**, 10.

Smithsonian Institution. 2006b. Montagu Island. *Bulletin of the Global Volcanism Network*, **31**, 3.

Smithsonian Institution. 2008. Montagu Island. *Bulletin of the Global Volcanism Network*, **33**, 7.

Smithsonian Institution. 2010a. Montagu Island. *Bulletin of the Global Volcanism Network*, **35**, 9.

Smithsonian Institution. 2010b. Heard Island. *Bulletin of the Global Volcanism Network*, **35**, 9.

Stephenson, J., Budd, G.M., Manning, J. & Hansbro, P. 2005. Major eruption induced changes to the McDonald Islands, southern Indian Ocean. *Antarctic Science*, **17**, 259–266.

Verwoerd, W.J., Russell, S. & Berruti, A. 1981. 1980 volcanic eruption reported on Marion Island. *Earth and Planetary Science Letters*, **54**, 153–156.

Vila, J., Marti, J., Ortiz, R., Garcia, A. & Correig, A.M. 1992. Volcanic tremors at Deception Island (South Shetland Islands, Antartica). *Journal of Volcanology and Geothermal Research*, **53**, 89–102.

Webley, P.W., Lopez, T.M., Ekstrand, A.L., Dean, K.G., Rinkleff, P., Dehn, J., Cahill, C.F., Wessels, R.L., Bailey, J.E., Izbekov, P. & Worden, A. 2012. Remote observations of eruptive clouds and surface thermal activity during the 2009 eruption of Redoubt volcano. *Journal of Volcanology and Geothermal Research*, 10.1016/j.jvolgeores.2012.06.023.

Wooster, J.J., Zhukov, B. & Oertel, D. 2003. Fire radiant energy for quantitative study of biomass burning: derivation from the BIRD experimental satellite and application to MODIS fire products. *Remote Sensing of Environment*, **86**, 83–107.

Wörner, G. & Viereck, L. 1989. The Mount Melbourne volcanic field (Victoria Land, Antarctica) I. *Field observations. Geologisches Jahrbuch,* **38**, 369–393.

Wright, R. & Pilger, E. 2008. Satellite observations reveal little interannual variability in the radiant heat flux from the Mount Erebus lava lake. *Journal of Volcanology and Geothermal Research*, **177**, 687–694.

Wright, R., Flynn, L.P., Garbeil, H., Harris, A.J.L. & Pilger, E. 2004. MODVOLC: near-real-time thermal monitoring of global volcanism. *Journal of Volcanology and Geothermal Research*, **135**, 29–49.